doi:10.1093/plphys/kiab244 PLANT PHYSIOLOGY 2021: 187: 133–157

Plant Physiology®

Research Article

Loss of *THIN EXINE2* disrupts multiple processes in the mechanism of pollen exine formation

Rui Wang [1] **and Anna A. Dobritsa** [1,*,†]

1 Department of Molecular Genetics and Center for Applied Plant Sciences, Ohio State University, Columbus, Ohio 43210

*Author for communication: dobritsa.1@osu.edu
†Senior author.

R.W. and A.A.D. conceived and designed the experiments, analyzed the data, and wrote the article. R.W. performed the experiments.
The author responsible for distribution of materials integral to the findings presented in this article in accordance with the policy described in the Instructions for Authors (https://academic.oup.com/plphys/pages/general-instructions) is: Anna Dobritsa (dobritsa.1@osu.edu).

Abstract

Exine, the sporopollenin-based outer layer of the pollen wall, forms through an unusual mechanism involving interactions between two anther cell types: developing pollen and tapetum. How sporopollenin precursors and other components required for exine formation are delivered from tapetum to pollen and assemble on the pollen surface is still largely unclear. Here, we characterized an Arabidopsis (*Arabidopsis thaliana*) mutant, *thin exine2* (*tex2*), which develops pollen with abnormally thin exine. The *TEX2* gene (also known as *REPRESSOR OF CYTOKININ DEFICIENCY1* (*ROCK1*)) encodes a putative nucleotide–sugar transporter localized to the endoplasmic reticulum. Tapetal expression of *TEX2* is sufficient for proper exine development. Loss of *TEX2* leads to the formation of abnormal primexine, lack of primary exine elements, and subsequent failure of sporopollenin to correctly assemble into exine structures. Using immunohistochemistry, we investigated the carbohydrate composition of the *tex2* primexine and found it accumulates increased amounts of arabinogalactans. Tapetum in *tex2* accumulates prominent metabolic inclusions which depend on the sporopollenin polyketide biosynthesis and transport and likely correspond to a sporopollenin-like material. Even though such inclusions have not been previously reported, we show mutations in one of the known sporopollenin biosynthesis genes, *LAP5/PKSB*, but not in its paralog *LAP6/PKSA*, also lead to accumulation of similar inclusions, suggesting separate roles for the two paralogs. Finally, we show *tex2* tapetal inclusions, as well as synthetic lethality in the double mutants of *TEX2* and other exine genes, could be used as reporters when investigating genetic relationships between genes involved in exine formation.

Introduction

To protect sperm cells and facilitate pollination, pollen surrounds itself with a complex, multi-layered cell wall. The outermost layer of the mature pollen wall is called exine. This is an unusual, non-carbohydrate-based cell wall comprised of the structurally rigid polymer, sporopollenin (Scott, 1994). Exine is often organized into intricate patterns, created through the precise deposition and assembly of its elements—baculae, which rise like columns from the pollen surface, and tectum, which forms a roof-like structure on top of the baculae (Erdtman, 1952, 1969; Scott, 1994). While this general description of exine architecture applies to pollen from many plant species, details of exine patterns often vary tremendously between species, possibly contributing to the efficiency and species specificity of pollination (Zinkl et al., 1999; Ariizumi and Toriyama, 2011). Although some aspects of exine development became better understood in recent years (e.g. enzymatic steps in the sporopollenin biosynthesis pathway and the general order and timing of events taking place on the surface of developing pollen

Received January 29, 2021. Accepted April 30, 2021. Advance access publication May 27, 2021

grains and in surrounding tissues; reviewed in Blackmore et al., 2007; Ariizumi and Toriyama, 2011; Quilichini et al., 2015; Shi et al., 2015; Wang and Dobritsa, 2018), many others, including how sporopollenin gets anchored to the pollen surface, how it assembles into exine, and what mechanisms govern exine patterning, remain essentially unknown.

Formation of exine begins after male meiosis, when four products of meiosis, the microspores, are kept in a tetrad configuration under the common callose wall (Owen and Makaroff, 1995; Quilichini et al., 2014a). At this stage, the prototypes of exine structures, probaculae and protectum, develop on the surface of each microspore. After the release of microspores from tetrads, these primary structures become converted into mature baculae and tectum through the deposition of large amounts of sporopollenin (or its precursors) transported from the nearby sporophytic tapetal cell layer. Before the mature exine develops, components and layout of the extracellular matrix surrounding developing microspores undergo dynamic changes, with several structures built and destroyed.

One such transient layer is primexine, which develops between the microspore plasma membrane and the callose wall. While poorly characterized, primexine is believed to play an essential role in the exine formation by providing a scaffold for the developing exine (Ariizumi and Toriyama, 2011; Lou et al., 2014). In several mutants of Arabidopsis (*Arabidopsis thaliana*) and rice (*Oryza sativa*) that lack exine development and display pollen lethality, these problems seem to originate from the defects in primexine formation (Paxson-Sowders et al., 1997, 2001; Ariizumi et al., 2004; Guan et al., 2008; Chang et al., 2012; Ma et al., 2013; Sun et al., 2013; Hu et al., 2014; Yu et al., 2016; Li et al., 2020; Mondol et al., 2020; Xu et al., 2020).

The chemistry of primexine could have a significant impact on exine formation. It has been proposed that components of primexine delivered to the pollen surface at the tetrad stage undergo phase separation, creating local chemical nano-environments that promote (self)-assembly of sporopollenin precursors into exine elements (Radja et al., 2019; Gabarayeva et al., 2020; Gabarayeva and Grigorjeva, 2021). While the precise chemical structure of primexine is unknown, it has long been believed to be carbohydrate-based and contain cell wall polysaccharides, such as cellulose, xylan, pectin, and structural glycoproteins (Heslop-Harrison, 1968; Rhee and Somerville, 1998; Majewska-Sawka and Rodriguez-Garcia, 2006). Changes in primexine composition caused by mutations may interfere with its ability to ensure proper exine development. This hypothesis is supported by the recent discoveries of several exine-patterning genes in Arabidopsis encoding proteins with homology to polysaccharide metabolism-related enzymes. Their mutants develop abnormal exine patterns in mature pollen grains, and some have confirmed abnormalities in the polysaccharide content of primexine. *SPONGY2/IRREGULAR XYLEM9-LIKE* (*SPG2/IRX9L*) and its homolog *IRX14L* encode xylosyltransferases involved in xylan backbone biosynthesis (Dobritsa et al., 2011; Li et al., 2017). *UNEQUAL PATTERN OF EXINE1/KAONASHI4* (*UPEX1/KNS4*) encodes a potential β-(1,3)-galactosyltransferase required for the biosynthesis of type II arabinogalactan for arabinogalactan proteins (AGPs) and/or the pectic polysaccharide rhamnogalacturonan I (Dobritsa et al., 2011; Suzuki et al., 2017). Through immunohistochemical analysis, the abnormal distribution of xylan, pectin, and AGPs was detected in the primexine of *spg2/irx9l* and *upex1/kns4*. Mutations in *SPONGY3/APYRASE7* (*SPG3/APY7*) lead to the abnormal exine patterning, similar to the *spg2/irx9l* phenotype (Dobritsa et al., 2011; Yang et al., 2013). *SPG3/APY7* encodes a putative nucleoside triphosphate-diphosphohydrolase, also known as apyrase, which, although not yet extensively characterized, has been proposed to function in carbohydrate-related processes (Yang et al., 2013). Some plant apyrases have been reported to function in the biosynthesis of glycoproteins, glycolipids, and cell wall polysaccharides, potentially by regulating transport of nucleotide-activated sugars into endomembrane compartments (Chiu et al., 2012; Lim et al., 2014). The similarity of its mutant exine phenotype to that of *spg2/irx9l* suggests that SPG3/APY7 might be involved in primexine formation.

In this study, we have focused on another gene, *THIN EXINE2* (*TEX2*), which is also essential for the formation of normal exine and likely has a carbohydrate-related function. We previously isolated a *tex2* mutant along with *spg2*, *spg3*, and *upex1* in a large-scale forward genetic screen in Arabidopsis (Dobritsa et al., 2011). Several mutant alleles of *TEX2* were described in that study and we showed that mutations in *TEX2* resulted in the development of unusually thin exine. Although we reported TEX2 as a putative nucleotide–sugar transporter (NST) at the time, since then the role of this gene in exine formation has not been further investigated.

More recently, another mutant allele of *TEX2* was isolated from a different genetic screen under the name of *repressor of cytokinin deficiency1-1* (*rock1-1*) and shown to act as a suppressor of cytokinin deficiency caused by the overexpression of cytokinin oxidase/dehydrogenase CKX1 (Niemann et al., 2015). This study revealed that TEX2/ROCK1 has functions aside from exine formation and highlighted the pleiotropic roles this protein plays in plant development. The TEX2 protein was found to localize to the endoplasmic reticulum (ER) in leaf and root cells, and the *rock1-1* mutation of *TEX2* showed the ability to decrease the activity of CKX1 by increasing its ER-associated protein degradation (ERAD; Niemann et al., 2015). The exact biochemical function of TEX2, however, remains a mystery.

Here, we characterize in detail the effect of the *tex2* mutations on pollen development and show that *TEX2* occupies an important place at the intersection of several pathways required for exine formation. We demonstrate that in anthers *TEX2* is expressed both in tapetum and developing microspores, its protein localizes to the ER in those cells, and *TEX2* expression in tapetum is sufficient for proper exine development. Loss of *TEX2* leads to abnormal primexine

layout, including increased accumulation of arabinogalactans, and subsequent failure of exine elements to assemble on the surface of released microspores. Through the use of immunolabeling, our study expands the understanding of primexine composition. We also show that one of the most prominent abnormalities in *tex2* anthers is the accumulation in tapetal cells of unusual metabolic inclusions, not previously reported for other exine mutants. We provide evidence that these inclusions likely correspond to sporopollenin precursors, which, in the absence of functional *TEX2*, fail to deposit on the microspore surface. We show that, in addition to *tex2*, at least one of the previously discovered exine mutants also accumulates similar inclusions. Finally, we demonstrate that these inclusions, as well as the presence/absence of synthetic pollen lethality in double mutants, can be utilized as reporters to help assemble the discovered exine genes into genetic pathways and networks.

Results

TEX2 is required for normal primexine formation and sporopollenin assembly on the microspore surface

To examine the effect of loss of *TEX2* on pollen wall development, we prepared ultra-thin cross sections of the wild-type and *tex2-3* anthers (see Supplemental Figure S1 for the diagram of the *tex2* mutations used in this study) at different developmental stages (Sanders et al., 1999) and imaged them with transmission electron microscopy (TEM; Figure 1). Development of the pollen wall begins at stage 7, when tetrads of microspores are produced. In the wild-type anthers at this stage, microspore plasma membrane starts undulating underneath the callose wall which surrounds each microspore in a tetrad, and the space between the plasma membrane and the callose wall becomes filled with primexine (Figure 1, A). Later in the tetrad stage, column-like probaculae and roof-like protectum start forming within the primexine matrix (Figure 1, B–D). At stage 8, free microspores with primary exine structures in place are released from tetrads, following the callose wall degradation (Figure 1, I).

In *tex2* anthers, plasma membrane undulation and primexine formation were observed after tetrad formation (Figure 1, E). However, in multiple independent preparations of *tex2*, the primexine matrix was more prominent and looked darker and coarser than in the wild type, and neither probaculae nor protectum formed within the *tex2* primexine during stage 7 (Figure 1, E–H). At stage 8, *tex2* microspores were released from tetrads without any primary exine structures on their surfaces (Figure 1, M).

At stage 9, major exine elements, tectum and baculae, gradually develop on the surface of wild-type microspores through further deposition of sporopollenin on the primary exine structures (Figure 1, J). During later stages, exine structures grow much longer and thicker, eventually producing the characteristic reticulate pattern of Arabidopsis exine (Figure 1, K and L). In contrast, *tex2* microspores at stage 9 became surrounded by small and round electron-dense granules that failed to attach to the microspore surface and instead appeared floating around the microspores (Figure 1, N and Supplemental Figure S2, N). These granules displayed electron density similar to that of the developing exine structures in the wild type, suggesting that the granules could be sporopollenin that failed to correctly anchor to and assemble on the microspore surface. At later stages, the granules somewhat enlarged but still did not assemble into exine structures (Figure 1, O and Supplemental Figure S2, O). In the mature *tex2* pollen grains, exine failed to develop the reticulate pattern and was significantly thinner than in wild-type pollen grains (Figure 1, P). The TEM results suggest that the thin-exine phenotype of *tex2* is likely caused by the abnormal formation of primexine followed by the lack of probaculae/protectum development during the tetrad stage, which, in turn, affects the assembly of exine structures at later stages.

Tapetum of *tex2* anthers accumulates abnormal inclusions

In addition to TEM, we also stained cross sections of resin-embedded anthers of the *tex2-3* allele at different developmental stages with toluidine blue and compared them with the similarly prepared wild-type anthers (Figure 2, A–L). No abnormalities were observed at this magnification in *tex2* at the early stages of development, up to and including the tetrad-containing stage 7 (Figure 2, G; compare with Figure 2, A). At stage 8, the processes of degradation of the callose wall around tetrads and release of individual microspores into the anther locules were also indistinguishable between wild type and *tex2* (Figure 2, B and H). However, at this stage the abnormal, blob-like inclusions first became noticeable in the *tex2* anthers (Figure 2, H, arrowheads). Such inclusions do not develop in the wild-type anthers (Figure 2, B), nor, to the best of our knowledge, have they been previously described for other exine mutants. The inclusions varied in size, with some being as large as cells, and were always found in the vicinity of tapetum. Inclusions showed no obvious cellular structures, and, while they were positive for toluidine blue staining, their cyan/aquamarine color was clearly distinguishable from the darker hue of tapetal cells, making inclusions easily recognizable. We used TEM to examine these inclusions in more detail and found that they were formed within tapetum, had amorphous appearance, and in many cases filled a large portion of tapetal cells, sometimes occupying entire cells (Figure 2, M and see Supplemental Figure S3 for additional examples). The abnormal inclusions were present in the *tex2* anthers throughout all the post-tetrad stages of development (Figure 2, H–L). At stage 12, after tapetal degeneration, inclusions remained in the locules among pollen grains (Figure 2, L and N). No other obvious differences in the development of non-sporogenic anther tissues were found in *tex2* (Figure 2, G–L).

In mature *tex2* flowers, the abnormal inclusions were visible with brightfield microscopy, without any staining, as

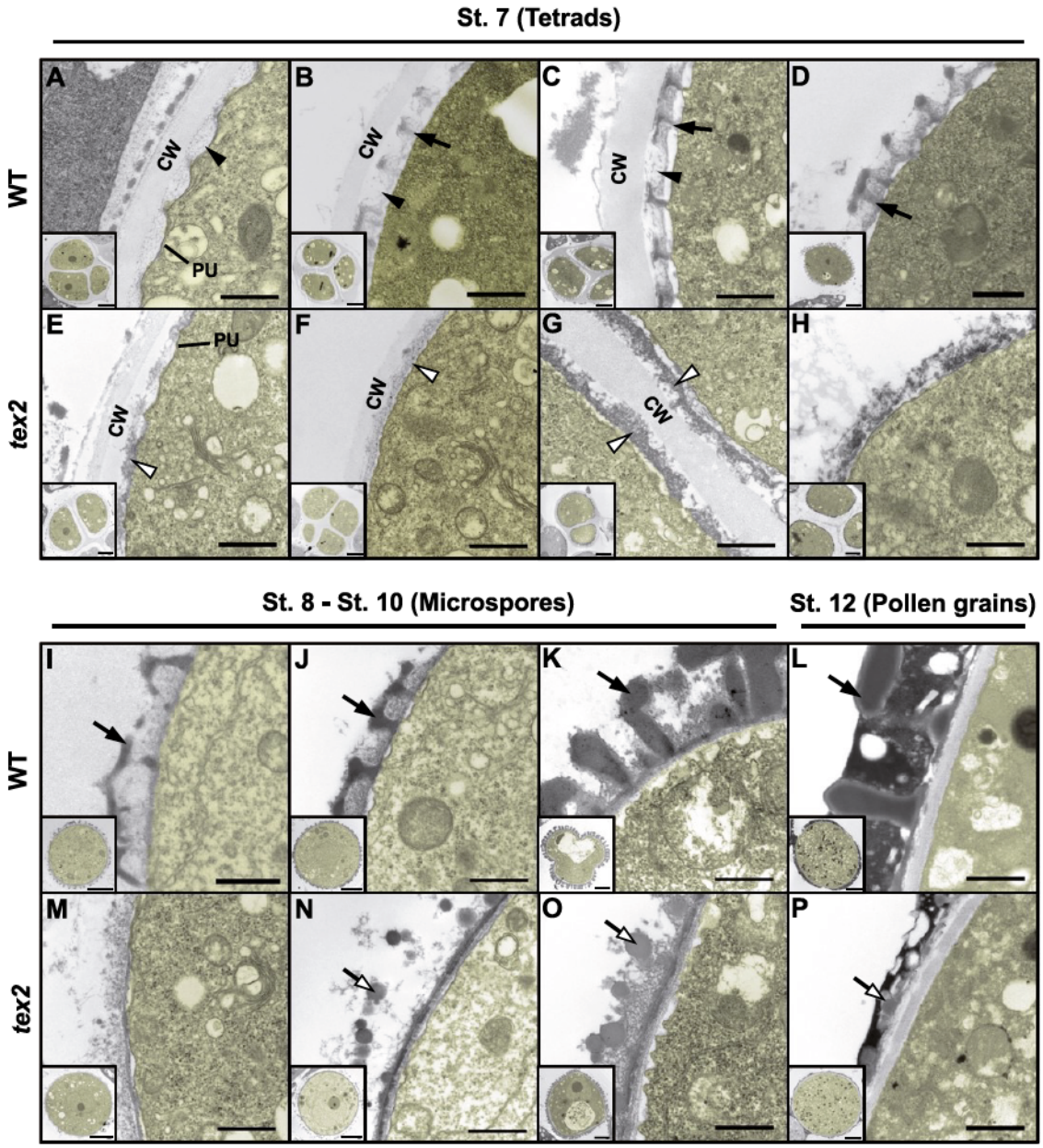

Figure 1 Formation of primexine and exine is affected during *tex2* pollen development. A–P, TEM micrographs of cross-sections of developing pollen from wild type (A–D, I–L) and *tex2* (E–H, M–P). Enlarged images show the details of cell surfaces from tetrads, microspores, and pollen grains. The views of cells from which the enlarged images were obtained are presented as insets at the bottom left to allow stage assignment; the larger versions of images shown in insets are available in Supplemental Figure S2. Images are arranged in order of pollen development from left to right. A–D, Formation of primexine (black arrowheads) and probaculae (black arrows) between the callose wall (CW) and the undulating microspore plasma membrane (PU) during the development of wild-type tetrads. E–H, The unusually coarse primexine (white arrowheads) was present, while the probaculae structures were absent during the *tex2* tetrad development. I–K, The developing exine structures (black arrows) on the surface of wild-type microspores. L, The mature exine structures (black arrow) on the surface of a wild-type pollen grain. M–O, Accumulation of granules (white arrows), likely representing unattached sporopollenin, around the *tex2* microspores. P, A very thin-exine layer (white arrow) was formed on the surface of *tex2* pollen grains. Cytoplasm of tetrads, microspores, and pollen grains is false-colored in yellow. Scale bars = 500 nm in (A–P) and 2.5 μm in the insets in (A–P).

brown spots among the pollen grains (Figure 2, P; compare with wild type in Figure 2, O). We further used scanning electron microscopy (SEM) to compare the mature anthers of wild type and *tex2* (Figure 3). The overall number of pollen grains found on the anther surface was similar for both genotypes (Figure 3, A, D, and G). However, their appearances were different. In the wild type, dehydrated pollen grains had an ellipsoid shape due to pollen folding inward along the three apertures, and their surface was covered with the characteristic reticulate exine (Figure 3, A–C). In the *tex2*

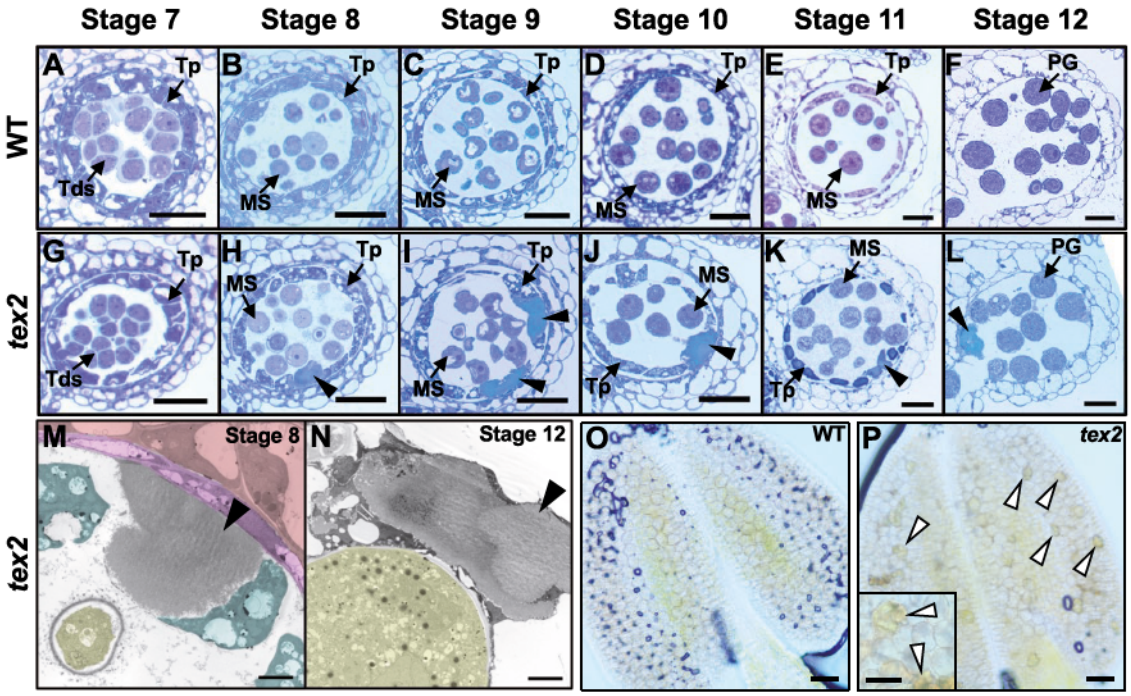

Figure 2 Abnormal inclusions in *tex2* anthers. A–L, Light micrographs of anther cross-sections of wild type (A–F) and *tex2* (G–L) from anther stage 7 to stage 12. G–L, The overall anther and pollen development in *tex2* is similar to wild type. However, after the tetrad stage, *tex2* anthers develop abnormal inclusions (arrowheads) associated with tapetum (H–K). After tapetum degenerates, the inclusions are released into locules (L). MS, microspore; PG, pollen grain; Tds, tetrads; Tp, tapetum. M and N, TEM images of the abnormal inclusions in *tex2* anthers at stages 8 and 12. M, An abnormal inclusion (arrowhead) is found within a tapetal cell at stage 8. Endothecium layer is false-colored in red, middle layer is false-colored in magenta, tapetum is false-colored in blue, and a microspore is false-colored in yellow. N, An abnormal inclusion (arrowhead) released into the locule after tapetum degeneration at stage 12. Pollen grain is false colored in yellow. O and P, Light micrographs of wild-type and *tex2* anthers mounted in glycerol. Abnormal inclusions (arrowheads) were identified as brown granules among pollen grains in *tex2* anthers after stage 12 (P). The inset shows *tex2* inclusions at higher magnification. Scale bars = 20 μm in (A–L), 2 μm in (M and N), 50 μm in (O and P), and 25 μm in the inset in (P).

mutants, thin exine no longer displayed the distinct reticulate pattern, and pollen grains showed disordered folding and irregular shapes, likely due to the loss of the normal structural support from exine (Figure 3, D–I). Intermixed with the *tex2* pollen on the anther surface was the abnormal inclusions (Figure 3, E, F, H, and I, arrowheads). They had irregular size and shape and had a much smoother surface than pollen grains, allowing them to be distinguishable from pollen.

These results indicate that the abnormal inclusions generated in tapetal cells after the tetrad stage represent a prominent abnormality of *tex2* anthers, likely directly connected to problems with exine development. As such, the inclusions might provide a clue to the function of the TEX2 protein and its role in exine formation.

Abnormal inclusions have multiple similarities with sporopollenin

Because the *tex2* pollen develops very thin exine and because the electron density of inclusions in TEM images is similar to that of sporopollenin assembling into exine on the pollen surface, we hypothesized that inclusions might be related to sporopollenin. To examine the nature of the *tex2* inclusions, we used several approaches (Figure 4). Alexander (1969) staining is commonly used to check pollen viability. With this method, viable pollen grains with normal protoplasm display dark-red or magenta color, while aborted pollen grains, which only have their walls, appear blue–green. (Although wall staining is also present in the wild-type pollen, it is largely masked by the color of the protoplasm.) In *tex2*, pollen grains all stained magenta, indicating their viability (Figure 4, A). At the same time, the abnormal inclusions in the anthers were stained bright blue–green, resembling the color of the pollen wall (Figure 4, A, arrowheads).

We then used acetolysis, a palynological technique in which pollen is treated with a concentrated mixture of acetic anhydrate and sulfuric acid. This treatment removes the cytoplasmic content of pollen but leaves the normal exine intact (Erdtman, 1960). We tested the sensitivity of the inclusions to this harsh treatment (Figure 4, B and C). Unlike *tex2* pollen grains, which are sensitive to acetolysis, the inclusions showed resistance to acetolysis (Figure 4, C).

We then used auramine O, a dye that displays strong fluorescence when bound to pollen exine. We found that, like exine, inclusions emitted strong fluorescence in the presence of this dye (Figure 4, D). While most of our experiments

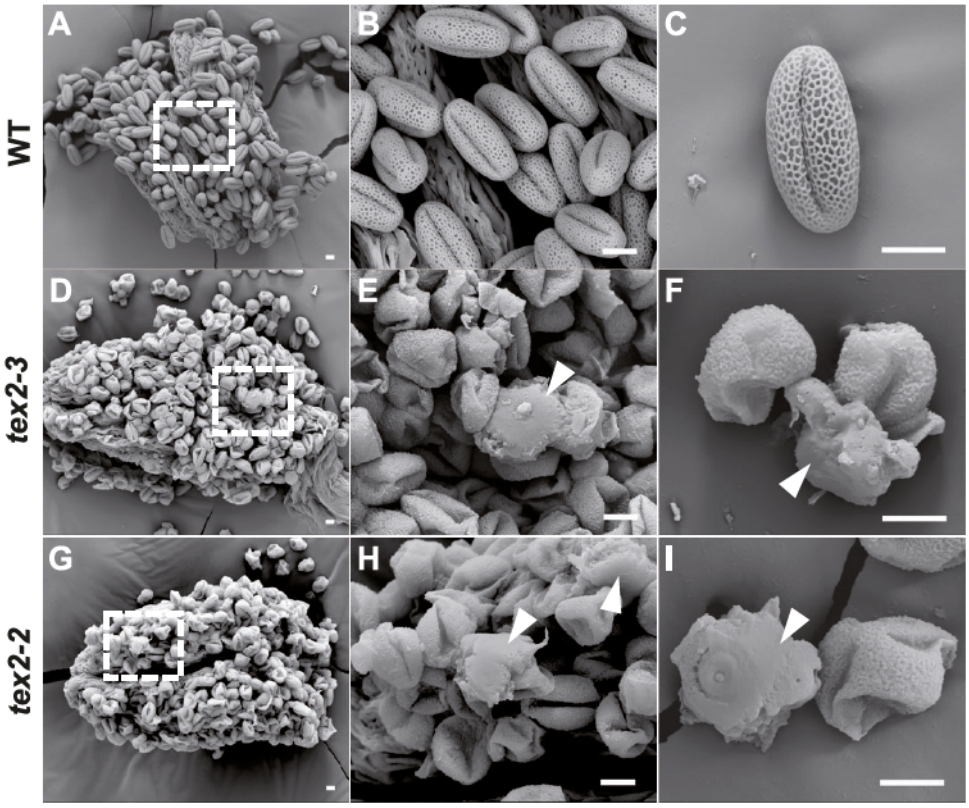

Figure 3 Abnormal inclusions are intermixed with pollen grains on the anther surface after dehiscence. A–I, SEM images of pollen grains and abnormal inclusions from wild type (A–C), *tex2-3* (D–F), and *tex2-2* (G–I). A, D, and G, The surface views of dehiscent anthers. B, E, and H, Magnified views of the boxed regions from (A), (D), and (G), respectively. The abnormal inclusions (arrowheads) in *tex2* anthers were present among pollen grains (E and H). C, F, and I, Surface views of individual dehydrated pollen grains and abnormal inclusions. The abnormal inclusions (arrowheads) are distinguishable by their smooth appearance from pollen grains in *tex2* anthers (F and I). Scale bars = 10 μm.

were done on the *tex2-3* allele, we also checked the *tex2-2* allele (Dobritsa et al., 2011; Supplemental Figure S1) for the presence of inclusions: the *tex2-2* anthers also contained inclusions visible with bright-field microscopy, Alexander staining, auramine O staining (Supplemental Figure S4), and SEM (Figure 3, G–I).

Pollen exine displays broad autofluorescence due to its chemical composition (Dobritsa et al., 2011; Roshchina, 2012; Quilichini et al., 2014b). Similar to exine, the abnormal inclusions also showed autofluorescence when excited by a 488-nm laser (Figure 4, E). To further characterize the *tex2* inclusions, we examined their autofluorescence spectrum and compared it with the spectra produced by exine walls in wild type and *tex2* (Figure 4, F). In this experiment, the top surfaces of abnormal inclusions and pollen grains were excited by a 405-nm laser, and their emission spectra were recorded in the interval of 410–620 nm. Both the wild-type exine and the thin exine of *tex2* showed similar spectra, consisting of a single peak with the maximum at 430 nm (Figure 4, F). Although the inclusions also produced a single-peak spectrum, its maximum shifted to 460–470 nm (Figure 4, F), suggesting that there are some differences in the composition of inclusions and exine. Taken together, these data suggest that, while not identical to exine, the *tex2* inclusions nevertheless share significant similarities with it and so might be composed of sporopollenin-like metabolites or sporopollenin precursors.

Accumulation of abnormal inclusions depends on the normal sporopollenin biosynthesis and transport

Sporopollenin biosynthesis occurs in tapetal cells (Ariizumi and Toriyama, 2011; Quilichini et al., 2015; Shi et al., 2015). Although not all details of this pathway have been elucidated, a number of genes encoding enzymes involved in this process were identified in Arabidopsis. Those include polyketide synthases *LESS ADHESIVE POLLEN5/POLYKETIDE SYNTHASE B* (*LAP5/PKSB*) and *LAP6/PKSA* (Dobritsa et al., 2010; Kim et al., 2010), cytochrome P450 enzymes *CYP704B1* and *CYP703A2* (Morant et al., 2007; Dobritsa et al., 2009), a fatty acyl reductase *MALE STERILITY2* (*MS2*; Aarts et al., 1997; Chen et al., 2011), *ACYL-COENZYME A SYNTHETHASE5* (*ACOS5*; de Azevedo Souza et al., 2009), and *TETRAKETIDE A-PYRONE REDUCTASES* (*TKPR1* and *TKPR2*; Grienenberger et al., 2010). Mutations in these genes cause abnormal exine formation and—in some cases—pollen lethality. While inactivation of *CYP704B1*, *CYP703A2*, and *MS2* (including their triple mutant combination) still allows

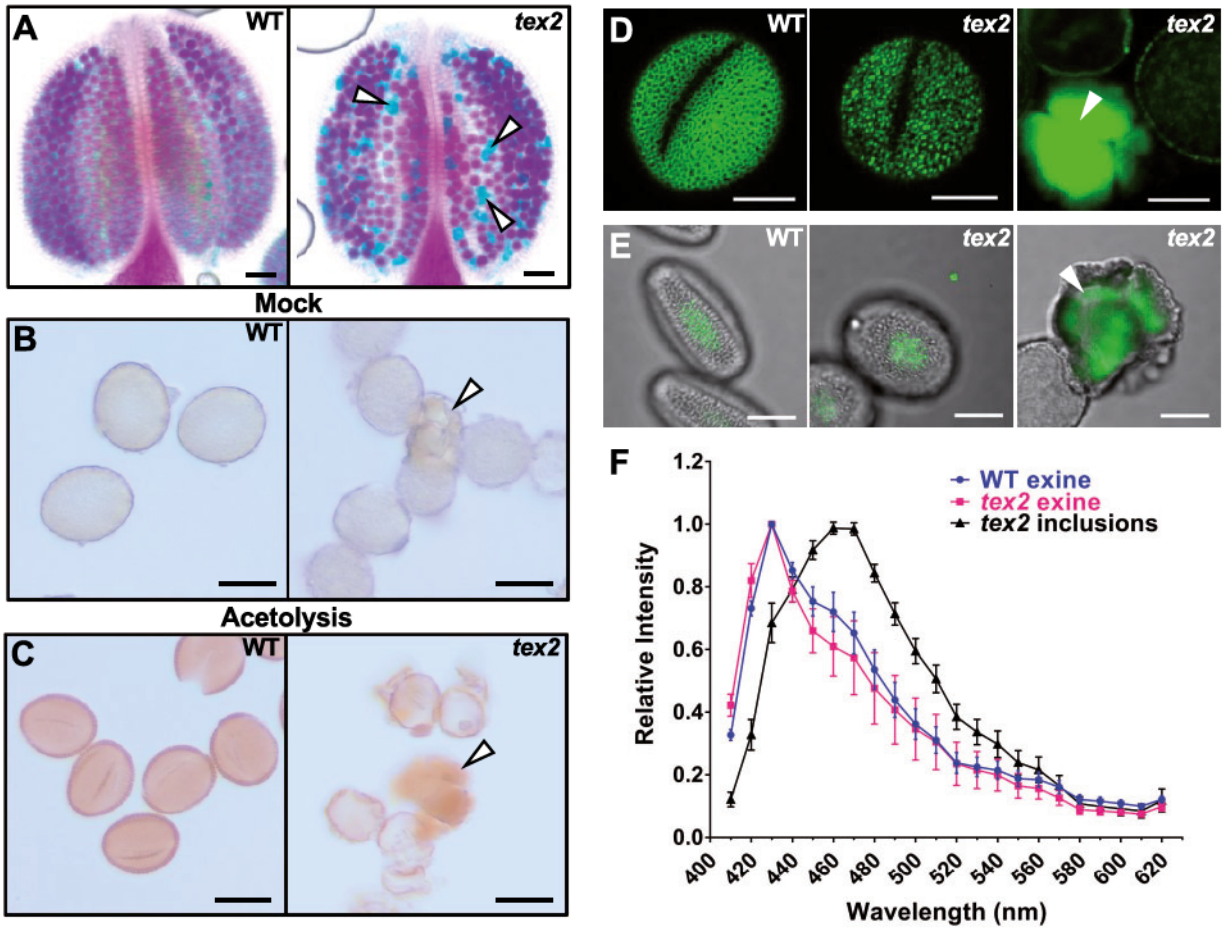

Figure 4 Characterization of the abnormal inclusions in *tex2*-3 anthers. A, Alexander's staining of wild-type and *tex2* anthers. The viable pollen grains were stained purple in both types of anthers, while abnormal inclusions (arrowheads) were stained blue in *tex2* anthers. B and C, Acetolysis analysis. Mock-treated (B) and acetolysis-treated (C) wild-type pollen grains, *tex2* pollen grains, and *tex2* abnormal inclusions (arrowheads). Wild-type pollen grains and abnormal inclusions showed resistance to acetolysis, whereas *tex2* pollen was lysed. D, Confocal images of the surface views of pollen exine and abnormal inclusions (arrowhead) from wild type and *tex2* that were stained with auramine O. E, Confocal images of autofluorescence (green) of wild-type exine, *tex2* exine, and abnormal inclusions (arrowhead) merged with brightfield images (gray). Autofluorescence was induced by a 488-nm laser. F, The autofluorescence spectra produced by the wild-type and *tex2* exines and *tex2* abnormal inclusions in response to the 405-nm excitation. The spectra were recorded in the 410-nm to 620-nm interval ($n = 20$ inclusions or grains per genotype). The autofluorescence data of individual abnormal inclusions and pollen grains were normalized, respectively, to the intensities of their 460-nm and 430-nm peaks. Error bars = SE. Scale bars = 50 μm in (A), 20 μm in (B and C), and 10 μm in (D and E).

pollen with almost no exine to survive (Dobritsa et al., 2009), the null mutations of *ACOS5* and *TKPR1* and the double *lap5 lap6* mutations lead to pollen lethality (de Azevedo Souza et al., 2009; Dobritsa et al., 2010; Grienenberger et al., 2010; Kim et al., 2010). In addition, mutations in *ATP-BINDING CASSETTE G26* (*ABCG26*), which encodes an ATP-binding cassette (ABC) transporter proposed to mediate the sporopollenin transport out of tapetum, also lead to the loss of exine formation and pollen death (Quilichini et al., 2010, 2014b; Choi et al., 2011; Dou et al., 2011).

To test if the accumulation of abnormal inclusions relies on the integrity of the sporopollenin biosynthesis and/or transport pathways, we created double mutants between *tex2* and the sporopollenin-disrupting mutants mentioned above. To visualize the presence of abnormal inclusions, we used Alexander staining (Figure 5, A–H). We found that when *tex2* was combined with *lap6*, *cyp704b1*, *cyp703a2*, *ms2*, *acos5*, *tkpr1*, or *abcg26*, the abnormal inclusions disappeared (Figure 5, A–F, and H). In contrast, the combinations of *tex2* with *tkpr2* (Figure 5, G) and *lap5* (described in detail below) did not suppress the formation of inclusions. In addition, the combinations of *tex2* with *cyp703a2*, *cyp704b1*, *lap6*, and *ms2*, which all produce viable pollen as single mutants (Figure 5, A–D, insets; Supplemental Figure S5), led to synthetic pollen lethality in the double mutants (Figure 5, A–D). This result demonstrates the existence of strong genetic interactions between *TEX2* and these sporopollenin genes, suggesting that *TEX2* might function in a pathway which is separate from the sporopollenin pathway but also

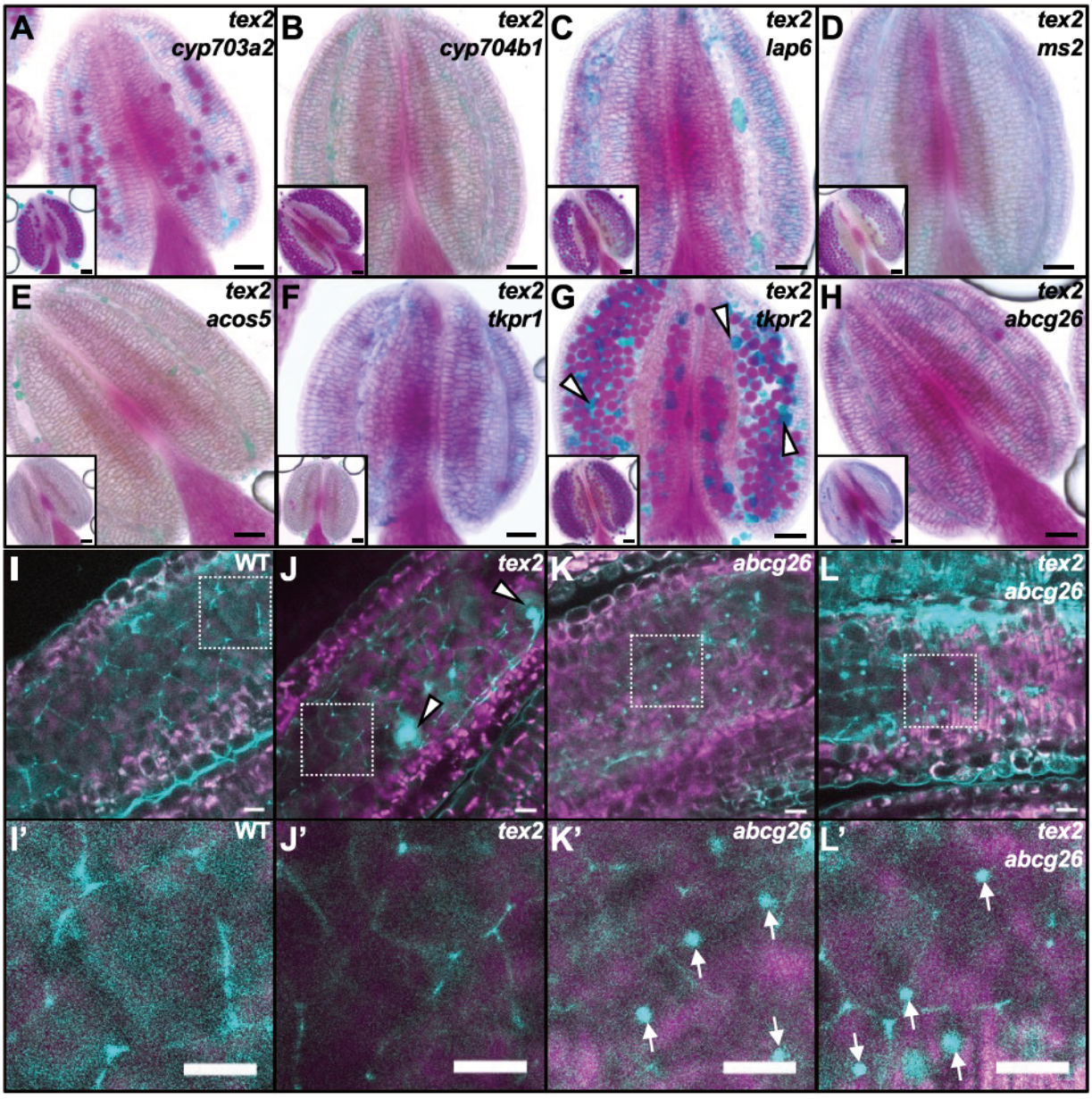

Figure 5 Accumulation of the *tex2* abnormal inclusions depends on sporopollenin metabolism and transport. A–H, Alexander's staining of anthers from the double mutants between *tex2* and the indicated mutants. The insets at bottom left show the anthers of the single mutants that were used for creating double mutants with *tex2*; the larger versions of images shown in insets are available in Supplemental Figure S5. *tex2* abnormal inclusions were absent in the double mutants of *tex2* and most sporopollenin-related mutants (A–F, H), with the exception of *tex2 tkpr2* (G, arrowheads). I–L′, Merged confocal images of the 405-nm-excited autofluorescence (cyan) from tapetal cells and chlorophyll autofluorescence (magenta) from non-tapetal cells in anthers with released microspores from wild type (I, I′), *tex2* (J, J′), *abcg26* (K, K′), and *tex2 abcg26* (L, L′). *tex2* inclusions are indicated by arrowheads in (J). I′–L′, Enlarged images of the boxed areas in (I–L), showing the auto-fluorescent inclusions (arrows) in the tapetal cells of *abcg26* (K′) and *tex2 abcg26* (L′). Scale bars = 50 μm in (A–H) and 10 μm in (I–L′).

needed for exine formation. In addition to Alexander staining, we also performed toluidine blue staining on cross sections of developing anthers in several of the double mutants that failed to accumulate inclusions in mature anthers (Supplemental Figure S6). These experiments confirmed that no inclusions were present in these double mutants at any stage of anther development and showed that the initial steps of pollen development (up to ~ stage 8) occurred normally. At later stages, microspores in these double mutants started undergoing degeneration; by stages 10 and 11, the anther locules became filled with debris, and by stage 12, no pollen remained (Supplemental Figure S6).

Since a majority of the double mutant combinations here resulted in pollen death, we wanted to rule out the possibility that the loss of inclusions in these double mutants was the consequence of the loss of pollen grains. To this end, we

generated double mutants between *tex2* and mutations in the genes *DEFECTIVE IN EXINE FORMATION1* (*DEX1*) and *NO EXINE FORMATION1* (*NEF1*) which are important for the formation of primexine and pollen viability but are not involved in the production of sporopollenin (Paxson-Sowders et al., 2001; Ariizumi et al., 2004). Although the anthers of *tex2 dex1* and *tex2 nef1* lacked pollen, they still accumulated inclusions (Supplemental Figure S7). (Note that the blue staining in the single *nef1* and *dex1* mutants is from the aborted pollen grains and not from the inclusions.) In addition, the combinations of double mutations in *TEX2* and several genes in the carbohydrate pathway (see below) also resulted in pollen death but did not suppress the accumulation of inclusions, further confirming that the presence of inclusions does not require pollen survival. Taken together, these genetic results indicate that accumulation of abnormal inclusions in *tex2* anthers depends on the normal biosynthesis and transport of sporopollenin in the tapetum.

Tapetal inclusions accumulating in the *abcg26* mutant are different from the *tex2* inclusions and do not require the TEX2 function

It was reported that a mutant in the putative sporopollenin transporter *ABCG26* also accumulates inclusions in tapetal cells, visible with the help of two-photon microscopy (Quilichini et al., 2014b). We adapted the approach of Quilichini et al. to traditional confocal microscopy, using a 405-nm laser for excitation, and found that this modified approach also allowed us to visualize the inclusions accumulating in the *abcg26* tapetal cells but not in the normal tapetum (Figure 5, I, I′, K, and K′, arrows), as well as the inclusions in the *tex2* tapetum (Figure 5, J, arrowheads). As previously described, the *abcg26* inclusions are small, never occupying much of the tapetal cell volume (Figure 5, K and K′), which makes them very different from the prominent *tex2* inclusions (Figure 5, J and J′). To check if the disruption of the *TEX2* function would affect the accumulation of the *abcg26* inclusions, we examined the tapetal cells of the *tex2 abcg26* double mutant with confocal microscopy. In agreement with the results of Alexander staining (Figure 5, H), the large *tex2* inclusions disappeared in the double mutant. However, the small *abcg26* inclusions were still present in *tex2 abcg26*, showing that the *abcg26* inclusions are independent of the *tex2* inclusions (Figure 5, L and L′). This result demonstrates that while the ABCG26 activity is necessary for accumulation of the *tex2* inclusions, the TEX2 activity is not needed for accumulation of the *abcg26* inclusions, suggesting that TEX2 (or the pathway in which it acts) is downstream of ABCG26.

tex2-like abnormal inclusions also accumulate in the *lap5* anthers

In previous studies, LAP5/PKSB was identified together with LAP6/PKSA (Dobritsa et al., 2010; Kim et al., 2010). Because these polyketide synthases are paralogs with 64% shared sequence identity, display similar patterns of expression and localization as well as similar *in vitro* activity, and because the phenotype of the double *lap5 lap6* mutant is much stronger than the phenotype of the single mutants, it was proposed that they function redundantly in sporopollenin biosynthesis (Dobritsa et al., 2010; Kim et al., 2010). However, in this study, we found that LAP5 behaves very differently from LAP6 in its genetic interactions with TEX2 and accumulation of inclusions in mutants. First, unlike the *lap6* mutation, which leads to the loss of pollen in the *tex2 lap6* double mutant, the loss of *LAP5* in the *tex2* background did not affect pollen viability (two *lap5* alleles were tested, with the same results; Figure 6, A and Supplemental Figure S8, D). Second, unlike the *lap6* mutation, the *lap5* mutation did not suppress the accumulation of inclusions in *tex2* (Figure 6, A, E–I, and O, and Supplemental Figure S8, C and D). Furthermore, we found that anthers of the *lap5* single mutants also accumulated the *tex2*-like inclusions (Figure 6, B, J–N, and P and Supplemental Figure S8, A and B). Like the *tex2* inclusions, the abnormal inclusions in *lap5* were resistant to acetolysis (Figure 6, R and S), stained with auramine O (Figure 6, T), showed autofluorescence when excited by a 488-nm laser (Figure 6, U), and produced the same autofluorescence spectrum when excited with a 405-nm laser (Figure 6, Q), indicating that the inclusions accumulating in *lap5* and *tex2* have similar characteristics. The accumulation of the abnormal inclusions in *lap5* and in *tex2 lap5* was suppressed in the presence of the *lap6* mutation (Figure 6, C and D). The differences in the phenotypes of *lap5* and *lap6* mutants revealed with the help of the *tex2* mutation suggest that these paralogs are not simply redundant. Therefore, LAP5 likely has a different function and/or occupies a different position from LAP6, possibly downstream, in the sporopollenin biosynthesis pathway.

These findings also prompted us to look more closely at the exine defects in *lap5*. We found that even though, as previously reported (Dobritsa et al., 2010; Kim et al., 2010), exine patterning was relatively normal in *lap5* pollen, its exine was thinner than the wild-type exine, thus resembling the *tex2* defect (Supplemental Figure S9, A–D). In the *tex2 lap5* double mutants, exine was affected more severely than in either of the single mutants (Supplemental Figure S9, E and F), with almost no sporopollenin present, indicating that even though similar tapetal inclusions accumulate in both cases, the two mutations likely disrupt different processes in exine formation.

TEX2 localizes to the ER in tapetum and microspores and its expression in tapetum is sufficient for proper exine formation

According to the publicly available RNA-seq data (Klepikova et al., 2016) and previous investigation of the *TEX2* promoter:*TEX2-GUS* expression (Niemann et al., 2015), TEX2 has a broad expression pattern and is expressed, among other tissues, in developing flower buds. To investigate the spatial–temporal expression pattern of *TEX2* during pollen development, we used the previously created construct

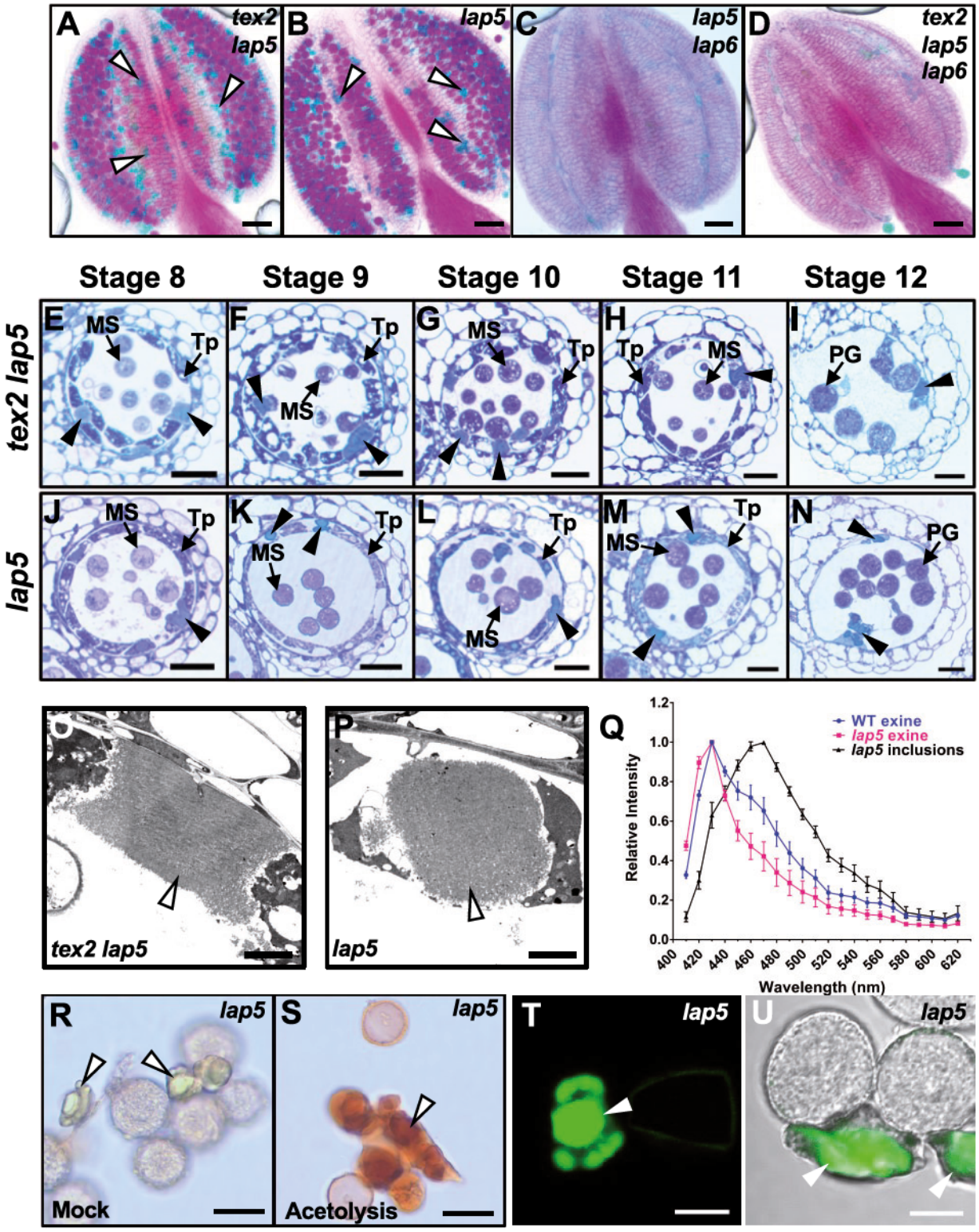

Figure 6 Accumulation of abnormal inclusions in *tex2* is not suppressed by the disruption of *LAP5*; *lap5* anthers also contain the *tex2*-like abnormal inclusions. A–D, Alexander staining of anthers from the indicated mutants. Accumulation of abnormal inclusions (arrowheads) was not affected in the *tex2 lap5* double mutant (A) (the GK_089C04 allele of *lap5* was used here; see also Supplemental Figure S8 for results on another *lap5* allele). *tex2*-like abnormal inclusions (arrowheads) were also present in *lap5* (B). Accumulation of abnormal inclusions in both *lap5* and *tex2 lap5* was suppressed by the *lap6* mutation (C and D). E–N, Light micrographs of anther cross-sections of *tex2 lap5* (E–I) and *lap5* (J–N) anthers from anther stage 8 to stage 12. The abnormal inclusions (arrowheads) in *tex2 lap5* and *lap5* anthers are associated with tapetum after the tetrad stage (E–H and J–M) and released into the locules after tapetum is degraded (I and N). O and P, TEM images of tapetal inclusions (arrowheads) in *tex2 lap5* and in *lap5*. Q, The autofluorescence spectrum produced by the *lap5* abnormal inclusions in response to the 405-nm excitation was recorded in the 410-nm to 620-nm interval and compared with the autofluorescence spectra generated by the wild-type and *lap5* exine ($n = 20$

ROCK1:ROCK1-GFPin (referred to here for consistency as P_{TEX2}:*TEX2-GFP*^{int}), in which *TEX2* was tagged internally with *GFP* and driven by its own promoter (Niemann et al., 2015). This construct complemented the effect of the *rock1-1* allele of *TEX2* on shoot development, indicating that it is functional (Niemann et al., 2015). After introgressing this construct into the *tex2-3* mutant, we confirmed that it was also able to function during pollen development and rescued the mutant exine phenotype in *tex2-3* (Figure 7, A–C). We also found that, like the other *tex2* alleles, *rock1-1* caused an abnormally thin exine, and that this defect was rescued by the P_{TEX2}:*TEX2-GFP*^{int} construct (Supplemental Figure S10), again verifying the functionality of this construct.

The earliest TEX2-GFP^{int} expression in anthers was found during the microspore mother cell (MMC) stage, when TEX2 was exclusively expressed in tapetum (Figure 7, E and E′). From the tetrad stage to the released microspore stage, TEX2-GFP^{int} was found in both tapetal cells and microspores (Figure 7, F–G′). After tapetal degradation, TEX2 was still expressed in maturing pollen grains (Figure 7, H and H′). These results demonstrate that during pollen development TEX2 is expressed in both gametophytic and sporophytic tissues.

Since the *tex2* inclusions accumulate specifically in tapetum, we tested if *TEX2* expression in that sporophytic tissue would be sufficient for its role in exine formation. To that end, we placed it under the control of the well-characterized tapetum-specific *A9* promoter (Paul et al., 1992; Feng and Dickinson, 2010). The resulting P_{A9}:*TEX2* construct was introduced into the *tex2* mutants and the phenotypes of 10 transgenic T_1 plants were examined. All transgenic plants produced pollen with normal exine (Figure 7, D), indicating that expression of *TEX2* in tapetum is sufficient for proper exine formation.

In both tapetal cells and developing microspores, the TEX2-GFP^{int} signal displayed a net-like subcellular localization pattern, with the fluorescent signal organized in a network around the nuclei (Figure 7, E′, F′, G′, and H′). This pattern is strongly reminiscent of the characteristic organization of ER. Supporting TEX2 as an ER resident protein, YFP-TEX2 expressed in *Nicotiana benthamiana* leaf epidermis colocalized with an ER marker (Supplemental Figure S11, A). In a previous study, an ER retention signal was identified at the C-terminus of TEX2 and it was suggested that the presence of GFP at the C-terminus of TEX2 masks this signal, allowing some C-tagged protein escape to the Golgi (Niemann et al., 2015). Consistently, we confirmed that TEX2 tagged with YFP at its C-terminus localized to both the ER and the Golgi (Supplemental Figure S11, B and C). Taken together, these results suggest that, like in vegetative tissues, in tapetum and microspores TEX2 localizes to the ER. We also found that, unlike the internally tagged TEX2, constructs in which TEX2 was tagged with YFP at the N- or C-terminus either did not produce clear YFP fluorescence or did not rescue the mutant phenotype (at least 10 T_1 lines were examined for each construct), indicating that presence of YFP at the protein termini interferes with the TEX2 function.

The UDP-GlcNAc transporter UGNT1 is unable to substitute for TEX2 in exine formation

Although TEX2 belongs to the NST family, its substrates remain unknown. Two studies tested TEX2 transport of variety of nucleotide sugars into microsomal or proteoliposomal vesicles in *S. cerevisiae* (Niemann et al., 2015; Ebert et al., 2018). The only nucleotide sugars that consistently showed significant increase in vesicles prepared from the *TEX2*-expressing yeast cells were UDP-*N*-acetylglucosamine (UDP-GlcNAc) and UDP-*N*-acetylgalactosamine (UDP-GalNAc). Yet, whether these nucleotide sugars serve as the main substrates for TEX2 is still debated (Niemann et al., 2015; Niemann and Werner, 2015; Ebert et al., 2018). While UDP-GlcNAc is used during the N-glycosylation of proteins and formation of plasma-membrane lipids glycosylinositol phosphorylceramides (Strasser et al., 2005, 2016; Ishikawa et al., 2018), there is currently no defined role for the GalNAc amino sugar moiety in plants. The ability of TEX2 to transport UDP-GlcNAc is much lower compared with that of another Arabidopsis NST, the Golgi-localized UGNT1, which was recently shown to be a *bona fide* UDP-GlcNAc transporter (Ebert et al., 2018). Also, addition of the GlcNAc sugar to proteins and lipids is believed to occur in the Golgi and not in the ER where TEX2 resides (Strasser, 2016; Ebert et al., 2018), casting more doubt on the role of TEX2 as a UDP-GlcNAc ER transporter.

Still, to investigate the possibility that TEX2 might be transporting UDP-GlcNAc during exine development, we attempted to test if the known UDP-GlcNAc transporter UGNT1 could substitute for the loss of TEX2 in exine formation. To this end, we placed the *UGNT1* gene under the control of the *TEX2* promoter. To guide the UGNT1 localization to the ER and not the Golgi, we also replaced its C-terminal cytoplasmic tail with that of TEX2 (Supplemental Figure S12, C), which contains the KKKKK sequence that fits with the consensus for the di-lysine-based ER retention signal and was previously shown to be important for TEX2 ER localization (Niemann et al., 2015). To account for the possibility that the N-terminal cytoplasmic tail of TEX2 may also

inclusions or grains per genotype). The auto uorescence data of individual abnormal inclusions and pollen grains were normalized, respectively, to the intensities of their 460-nm and 430-nm peaks. Error bars = SE. R and S, The abnormal inclusions in *lap5* (arrowheads) are resistant to acetolysis. *lap5* pollen grains and inclusions after mock treatment (R) and acetolysis treatment (S). T, Confocal image of *lap5* abnormal inclusions (arrowheads) stained with auramine O. U, Merged image of the 488-nm-induced auto uorescence of the *lap5* abnormal inclusions (green, arrowheads) and the bright eld image (gray). MS, microspore; PG, pollen grain; Tp, tapetum. Scale bars = 50 μm in (A–D), 20 μm in (E–N, R, and S), 2 μm in (O and P), and 10 μm in (T and U).

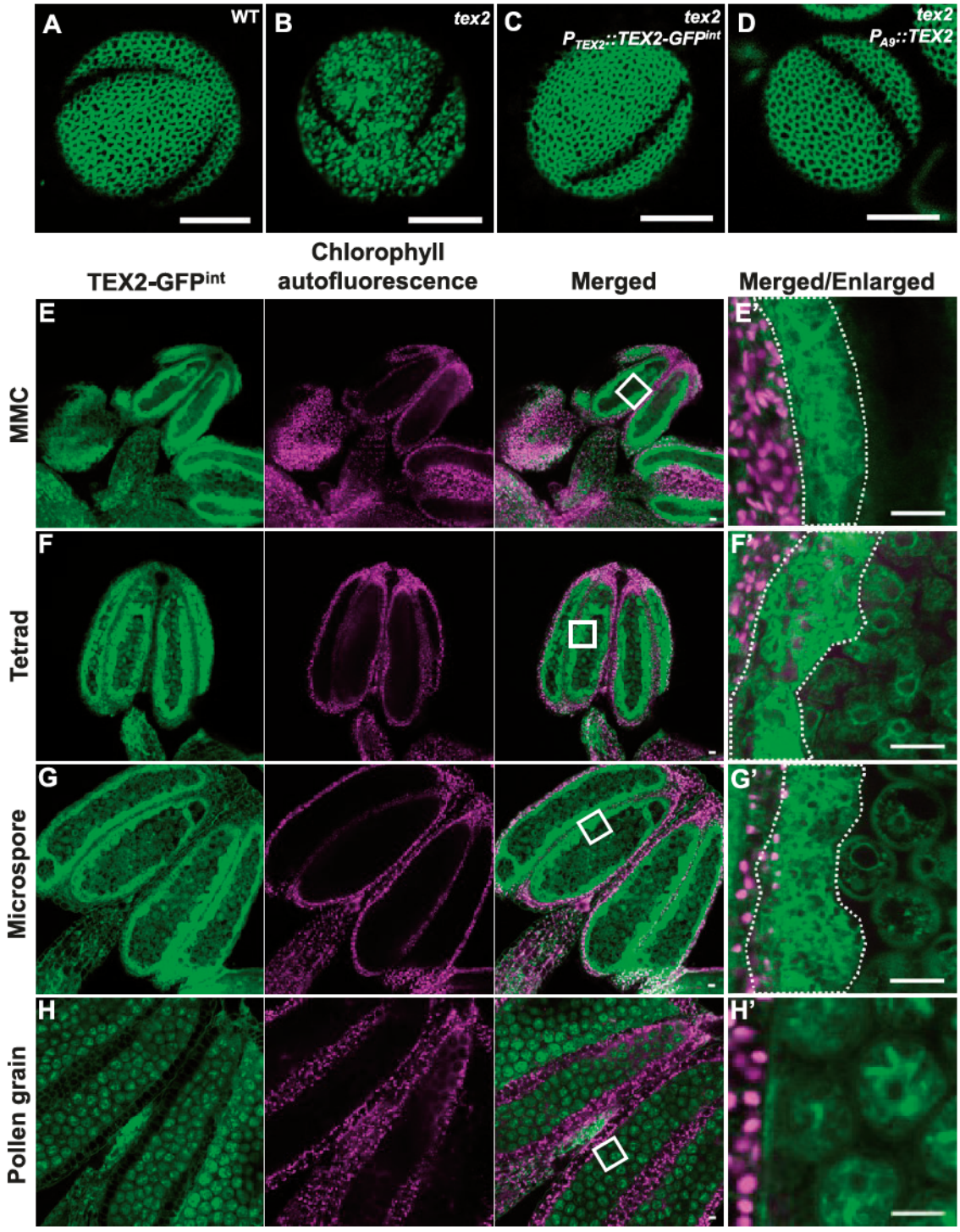

Figure 7 TEX2-GFP^{int} is expressed in tapetum, tetrads, microspores, and pollen grains. A–D, Confocal images of the auramine O-stained pollen grains from the wild-type (A), *tex2* (B), transgenic *tex2* plants expressing P_{TEX2}::*TEX2-GFP*^{int} (C), and P_{A9}::*TEX2* (D). E–H, Confocal images of the signal produced by TEX2-GFP^{int} driven by the *TEX2* promoter in *tex2* anthers of different developmental stages. E, Anther at the MMC stage. F, Anther at the tetrad stage. G, Anther at the released microspore stage. H, Anther containing pollen grains. E′–H′, Enlarged images of the boxed areas from (E–H), showing the details of the subcellular fluorescent pattern of TEX2-GFP^{int}. Tapetum is outlined with dashed lines. Scale bars = 10 μm.

carry some signal, we created another construct in which both the N- and C-terminal cytoplasmic tails of UGNT1 were replaced with those of TEX2 (Supplemental Figure S12, D). Both chimeric constructs along with the unmodified *UGNT1* under the *TEX2* promoter were then transformed into the *tex2* mutant, and we assessed their ability to rescue the mutant exine. None of the constructs, however, was able to restore the wild-type exine ($n = 8$ T_1 plants for each

construct), suggesting that TEX2 is unlikely to transport UDP-GlcNAc into the tapetal ER to promote exine formation.

tex2 primexine shows abnormal accumulation of arabinogalactans

Given that the earliest defect detected on the pollen surface was the abnormal formation of the primexine matrix, we took a closer look at this structure. Although the exact composition of primexine is unknown, the available evidence suggests that it is made of polysaccharide-based materials (Heslop-Harrison, 1968; Rhee and Somerville, 1998; Majewska-Sawka and Rodriguez-Garcia, 2006). Several exine patterning genes, such as *SPG2/IRX9L*, *IRX14L*, and *UPEX1/KNS4*, were previously found to encode enzymes likely involved in polysaccharide metabolism (Dobritsa et al., 2011; Li et al., 2017; Suzuki et al., 2017). The mutants of these genes, which encode glycosyl transferases, showed abnormalities in the primexine layout and/or composition. We hypothesized that the abnormal primexine in *tex2* might also have changes in its polysaccharide composition. To test this hypothesis, we embedded the tetrad-containing anthers in LR White resin and stained their cross sections with monoclonal antibodies (mAbs) directed against several types of plant cell-wall glycans (Figure 8 and Supplemental Figure S13). We also used Calcofluor White to label the callose walls surrounding tetrads, as well as cell walls of the sporophytic anther layers.

To detect xylan epitopes, which were previously identified as constituents of primexine, we used LM10 and LM11 mAbs (McCartney et al., 2005; Li et al., 2017; Xu et al., 2020). In both wild type and *tex2*, the LM10 and LM11 signals were observed in the primexine and were indistinguishable between the two genotypes (Figure 8, A and G, B and H). For both genotypes, the LM11 signal was consistently stronger than that of LM10.

We then used JIM5 and JIM7 mAbs to label pectin. JIM5 binds to non-methylesterified or sparsely methylesterified homogalacturonans, while JIM7 binds to relatively heavily methylesterified homogalacturonans (Knox et al., 1990; Willats et al., 2000; Clausen et al., 2003; Verhertbruggen et al., 2009). Neither JIM5 nor JIM7 labeling was affected in *tex2* compared with wild type (Figure 8, C and I, D and J). JIM5 labeling was present specifically in primexine (Figure 8, C and I), while JIM7 labeling was also found in the area corresponding to the primary cell wall outside the callose wall (the remnant of the wall surrounding the MMC), as well as in the walls of other anther cell layers (Figure 8, D and J).

Another type of polysaccharides predicted to exist in primexine is the AGPs, a diverse class of surface proteoglycans (Majewska-Sawka and Rodriguez-Garcia, 2006; Suzuki et al., 2017). Multiple antibodies were created that can bind to the polysaccharide epitopes of AGPs (Knox et al., 1991; Pennell et al., 1991; Yates et al., 1996; Pattathil et al., 2010). To look at the arabinogalactan distribution in the wild-type and *tex2* primexines, we tested the JIM4, JIM8, JIM13, JIM15, JIM17, JIM20, and MAC207 mAbs. In wild-type tetrads, JIM8, JIM15, JIM20, and JIM13 labeling was detected mainly in the primary maternal cell wall surrounding each tetrad, and not around individual microspores in a tetrad (Figure 8, E and F and Supplemental Figures S13, C and E, S14, A and C). Similar patterns were observed in *tex2* with JIM20 and JIM13 mAbs (Supplemental Figure S13, I and K). In contrast, the JIM8 and JIM15 signals in *tex2* were consistently reduced in the primary maternal cell wall, but instead appeared around individual microspores, at the position corresponding to primexine (Figure 8, K and L and Supplemental Figure S14, B and D). No JIM4, JIM17, or MAC207 labeling was found in either the wild-type or *tex2* tetrads (Supplemental Figure S13, A, B, D and G, H, J). Taken together, the immunolabeling results indicate that the arabinogalactan epitopes recognized by JIM8 and JIM15 accumulate at higher-than-normal levels in the *tex2* primexine and at reduced levels in the *tex2* primary maternal wall, whereas the distribution of xylan and pectin is not affected by the *tex2* mutation.

A strong genetic interaction exists between *TEX2* and some of the carbohydrate-related exine-patterning genes

Since several genes required for normal exine patterning and encoding enzymes which might be involved in carbohydrate metabolism were recently identified (Dobritsa et al., 2011; Yang et al., 2013; Li et al., 2017; Suzuki et al., 2017), we tested their genetic interactions with *TEX2* (Figure 9). The double mutants of *tex2* with *spg2/irx9l* and *irx14l*, which affect glycosyl transferases involved in xylan biosynthesis, displayed a dramatic loss in pollen viability, similar to the effect of mutations in the sporopollenin-related genes (Figure 9, A and B, compare with anthers from single carbohydrate-related exine mutants shown as insets and in Supplemental Figure S15). We also observed a similar effect in the double mutant between *tex2* and the *spg3* mutation, which affects the *APY7* gene encoding an apyrase (Dobritsa et al., 2011; Yang et al., 2013) that might also be involved in the biosynthesis of complex carbohydrates (Figure 9, C and Supplemental Figure S15). Yet, unlike the mutations in the sporopollenin-related genes, the mutations in the carbohydrate-related genes did not suppress the accumulation of the abnormal inclusions in the *tex2* anthers (Figure 9, A–C and Supplemental Figure S16), confirming that the loss of pollen does not automatically lead to a failure to accumulate inclusions, as well as indirectly supporting the notion that inclusions likely represent the abnormal build-up of sporopollenin-like molecules, which should not be affected by the mutations used here.

Finally, to further explore the connection between TEX2 and arabinogalactans, we also created a double mutant between *tex2* and the mutant that affects the exine patterning gene *UPEX1/KNS4*, which encodes a β-1,3-galactosyl transferase predicted to be involved in the formation of arabinogalactans on the microspore surface (Dobritsa et al., 2011; Suzuki et al., 2017). This combination of mutations did not

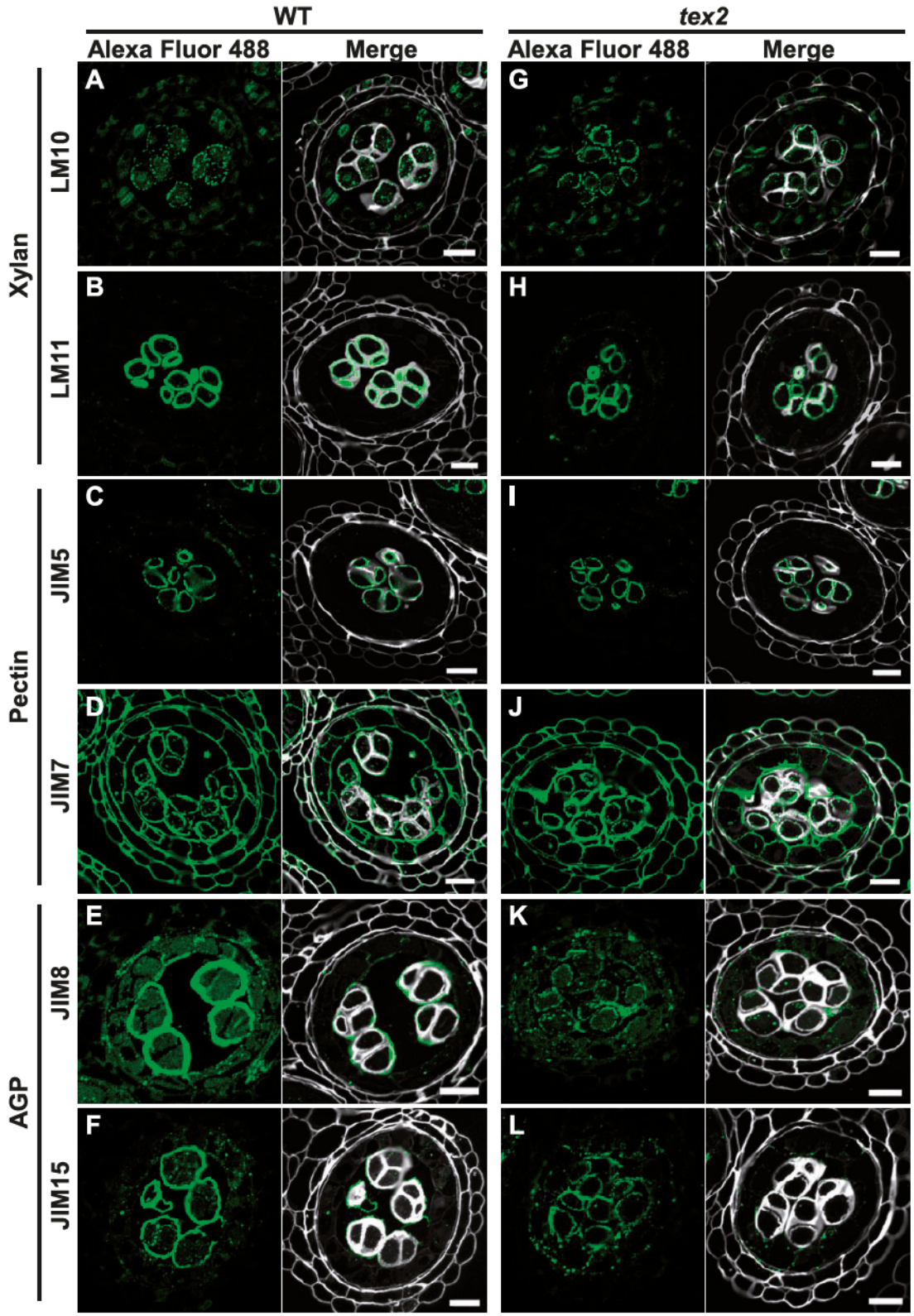

Figure 8 Distribution of several cell wall polysaccharides in tetrads. A–L, Confocal images of anther cross-sections containing tetrads of wild type (A–F) and *tex2* (G–L). Anthers were embedded in LR White resin and sections were immunolabeled with the indicated antibodies. Alexa Fluor 488 antibody was used as the secondary antibody for polysaccharide immunolabeling (green). The sections were also stained with Calcofluor white and imaged separately (white), then merged with immunolabeling images. Scale bars = 10 μm.

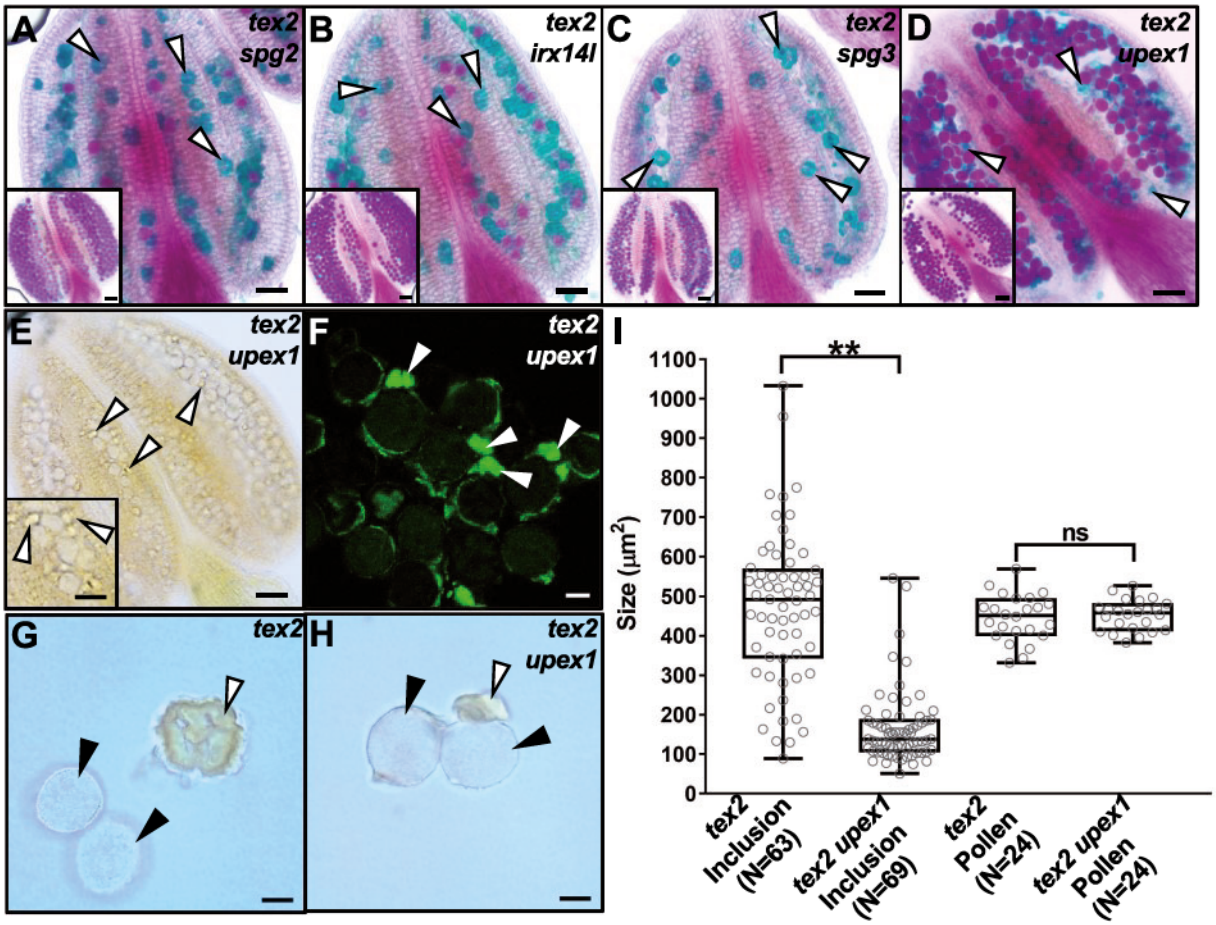

Figure 9 Genetic interactions were observed between *TEX2* and several carbohydrate-related exine-patterning genes. A–D, Alexander staining of anthers from the indicated double mutants. The insets show anthers from the corresponding single mutants of the carbohydrate-related exine-patterning genes (larger versions of these images are available in Supplemental Figure S16). Pollen lethality was observed in the double mutants of *tex2 spg2* (A), *tex2 irx14l* (B), and *tex2 spg3* (C), suggesting a strong genetic interaction between *TEX2* and these genes. *tex2* abnormal inclusions are indicated by white arrowheads. Pollen viability was not affected in *tex2 upex1*, but abnormal inclusions (white arrowheads) looked smaller than in *tex2* and other double mutants. E, Light micrograph of *tex2 upex1* anther mounted in glycerol. Abnormal inclusions (white arrowheads) were identified as brown granules among pollen grains in *tex2 upex1* anthers after stage 12. The inset shows inclusions at higher magnification. F, Confocal image of *tex2 upex1* abnormal inclusions (white arrowheads) stained with auramine O. G and H, Light micrographs of pollen grains (black arrowheads) and inclusions (white arrowheads) from dehiscent anthers of *tex2* (G) and *tex2 upex1* (H). I, Box plots showing the size measurements of pollen grains and inclusions from *tex2* and *tex2 upex1*. The top and bottom of the box represents the 25 and 75 percentiles. The line in the middle of the box indicates the median. The top and bottom bars represent the maximum and minimum. Asterisks indicate significant differences of the inclusion size between *tex2* and *tex2 upex1* mutants based on Student's *t* test (**$P < 0.01$; ns, not significant). Scale bars = 50 μm in (A–E), 25 μm in the inset in (E), and 10 μm in (F–H).

affect pollen viability (Figure 9, D), demonstrating that *TEX2* does not genetically interact with *UPEX1/KNS4* in the same way it does with the other carbohydrate-related genes studied here. We also examined exine in *tex2 upex1* with auramine O staining. In this double mutant, exine appeared to be more severely disrupted than in either of the single mutants (Supplemental Figure S17), although not to the same extent as in *tex2 lap5*.

Interestingly, although the mutation in *UPEX1/KNS4* did not completely suppress the accumulation of the *tex2* inclusions, the inclusions became noticeably smaller in the double mutant compared with the *tex2* mutant (Figure 9, E–I). Given that *tex2* and *upex1/kns4* have potentially opposite effects on the accumulation of arabinogalactans in primexine, this might suggest that the reduction of these compounds in primexine or elsewhere due to the loss of *UPEX1/KNS4* may partially rescue the accumulation of sporopollenin-like products as abnormal inclusions in *tex2*.

To examine how the single *upex1/kns4* mutation and the *tex2 upex1/kns4* double mutations affect the formation and distribution of arabinogalactans in the developing tetrads, we stained the sections of tetrad-stage anthers from the corresponding mutants with JIM8 and JIM15 antibodies. Compared with the signals in wild-type and *tex2* anthers included as controls on the same slides (Figure 10, A, B, E, and F and Supplemental Figure S14, E, F, I, and J), the signals in both *upex1/kns4* and *tex2 upex1/kns4* were much weaker, in agreement with the reduction of arabinogalactans in the

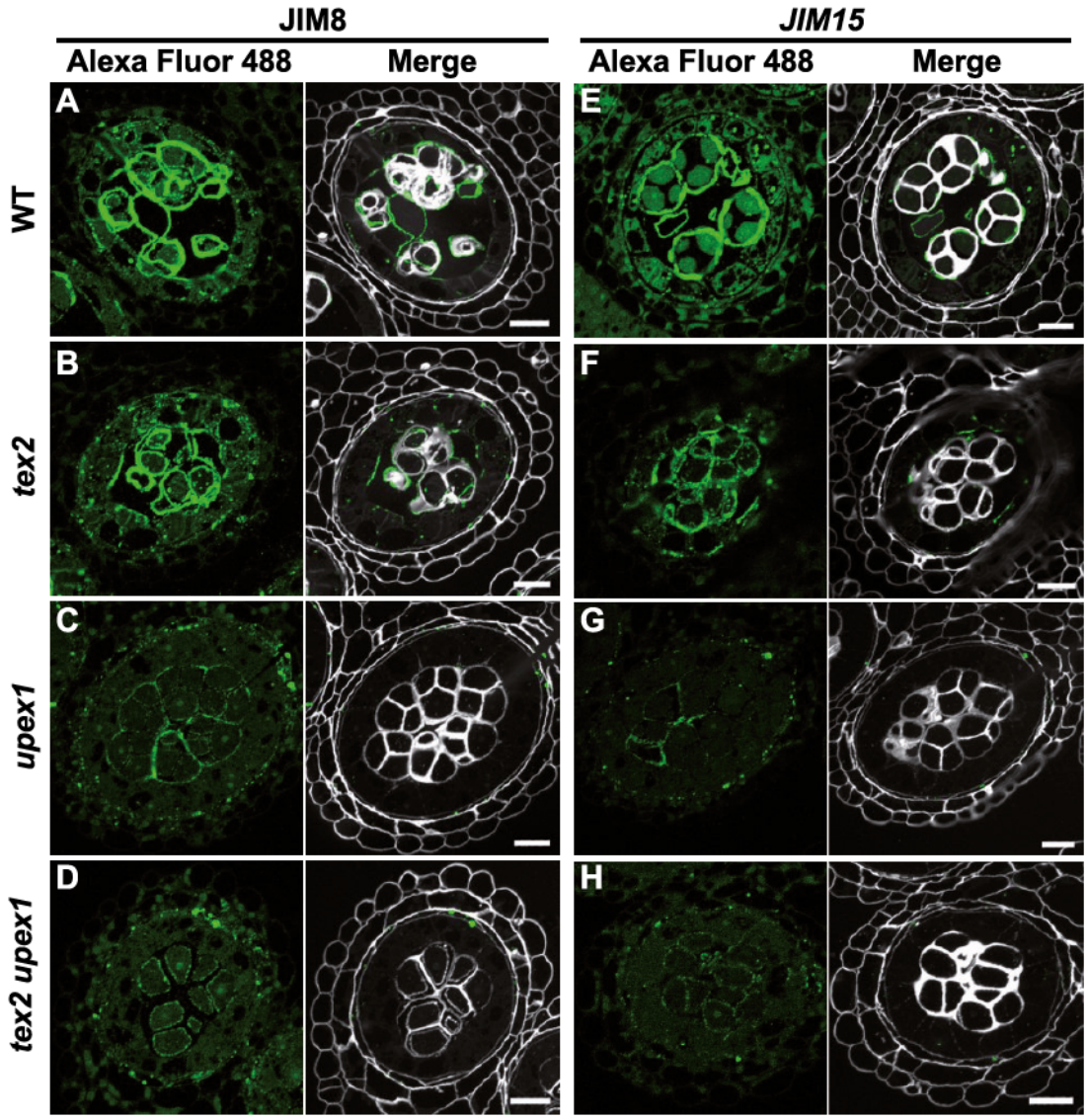

Figure 10 Distribution of AGPs in tetrads of *upex1* and *tex2 upex1*. A–H, Confocal images of anther cross-sections containing tetrads of wild type (A and E), *tex2* (B and F), *upex1* (C and G), and *tex2 upex1* (D and H). Anthers were embedded in LR White resin and sections were immunolabeled with the indicated antibodies. Alexa Fluor 488 antibody was used as the secondary antibody for the AGP signal observation (green). The sections were also stained with Calcofluor white and imaged separately (white), then merged with immunolabeling images. Scale bars = 10 μm. See Supplemental Figure S14 for enlarged versions of tetrads shown here.

absence of the UPEX1/KNS4 function (Figure 10, C, D, G, and H and Supplemental Figure S13, G, H, K, and L). Notably, however, when the arabinogalactan signals were compared between the last two genotypes, the signal in the *tex2 upex1/kns4* primexine was consistently stronger than the signal in the *upex1/kns4* primexine (Figure 10, B, D, F, and H and Supplemental Figure S14, E–L), again providing evidence that the loss of *TEX2* increases the accumulation of arabinogalactans in primexine at the tetrad stage.

Discussion

TEX2 is required for proper primexine formation

Primexine, the ephemeral and poorly characterized matrix that briefly occupies the ~100-nm space between the callose wall and the plasma membrane of developing microspores, is believed to play an important role in the formation of pollen exine. In this study, we provided a detailed view of pollen wall development in *tex2*, an Arabidopsis mutant whose defects in exine formation appear to stem from the abnormal formation of primexine. By imaging pollen wall structures in *tex2* and wild type with high resolution at specific time points over the course of pollen development, we obtained a comprehensive view showing how sporopollenin in *tex2* fails to be deposited on the surface of developing microspores for assembly into exine.

The tetrad stage is known for its fundamental role in pollen wall development: multiple events happen during that stage and several structures are rapidly sequentially built on the microspore surface (Ariizumi and Toriyama, 2011; Wang and Dobritsa, 2018). By capturing the views of the

wall structures with TEM at different time points of the tetrad stage, we were able to walk through the timeline of events happening underneath the callose wall in wild type and *tex2*. In *tex2*, although the plasma membrane undulation happens normally and primexine develops, this primexine appears darker and coarser compared with its wild-type counterpart. Recently, it has been proposed that components of primexine might undergo phase separation to create conditions necessary for the formation of exine structures (Radja et al., 2019; Gabarayeva et al., 2020; Gabarayeva and Grigorjeva, 2021). Intriguingly, the *tex2* primexine looks much more homogenous than the wild-type primexine, suggesting phase separation of primexine components might not be occurring properly in *tex2*. The defects in formation of primexine in *tex2*, in turn, appear to preclude the formation of the earliest elements of the future exine pattern, probaculae and protectum. With no primary exine structures, the accumulation of sporopollenin at the microspore surface in the post-tetrad period is largely prevented, resulting in the thin exine, characteristic of the *tex2* mature pollen. We have observed some unassembled sporopollenin aggregating into small granules that fail to anchor at the microspore surface and instead float around the developing microspores. These findings suggest that changes in *tex2* primexine disrupt its ability to provide a proper environment for the subsequent steps in exine formation.

Primexine carbohydrate composition is affected in *tex2*

Our detailed analysis of primexine development in *tex2*, combined with the potential carbohydrate-related function of the TEX2 protein, suggests a possible change in the polysaccharide composition in the *tex2* primexine. Primexine has long been thought to contain polysaccharides. Yet, because primexine is produced in tiny amounts and present only for a short time, its composition has been very challenging to study. Immunohistochemistry is currently one of the best methods for characterizing cell wall components *in situ* within plant tissues (Pattathil et al., 2010; Ruprecht et al., 2017). In this study, we used immunolabeling with plant cell wall glycan-directed mAbs to test the distribution of cell wall glycans in primexine, with a focus on the tetrad stage.

Using LM10 and LM11 mAbs, we found abundant xylan in both wild-type and *tex2* primexines at the tetrad stage. This timing is earlier than in a previous study, which suggested that xylan does not appear in primexine until the free microspore stage (Li et al., 2017). Similarly, we observed the labeling for both sparsely methylesterified pectin (with JIM5 mAb) and more heavily methylesterified pectin (with JIM7 mAb) in primexines of wild type and *tex2* during tetrad development. Again, this finding pushes the time when these compounds first accumulate in primexine to an earlier point than previously appreciated (Suzuki et al., 2017). Better understanding of the advent of different compounds in tetrad-stage primexine is crucial, since by the time microspores are released from tetrads, they already contain the primary exine structures. No difference between wild type and *tex2* was detected for xylan and pectin distribution in primexine or the timing of their first appearance.

For arabinogalactans, we used multiple mAbs. Among those that produced signal in tetrads, the staining generated by JIM8, JIM13, JIM15, and JIM20 in the wild-type tetrads was concentrated in the area that corresponds to the primary cell wall of the original mother cell and not in the primexine. The same labeling pattern was observed with JIM13 and JIM20 in *tex2*. However, the JIM8 and JIM15 labeling patterns differed in *tex2* from the wild type: in *tex2*, the epitopes recognized by these two mAbs decreased significantly in the area of the primary cell wall around the mutant tetrads, but instead appeared around individual microspores, indicating that arabinogalactans recognized by these antibodies accumulated in the *tex2* primexine. The simultaneous decrease of the JIM8/JIM15 signal in the primary cell wall could indicate that the compounds recognized by these mAbs in this region represent materials produced in the tapetum, which are in the process of passing through the cell wall layers surrounding tetrads on their way to the microspore surface. If the loss of TEX2 compromises those external layers, this might allow these compounds an easier access to the primexine area, resulting in their increased accumulation there. The exact epitopes recognized by JIM8 and JIM15 in AGPs are unknown, but these mAbs have been previously placed in the same anti-AG clade, AG-3 (out of four total), based on their similar binding specificity to a panel of carbohydrates in ELISA (Pattathil et al., 2010). In contrast, JIM13 and JIM20 have been placed, respectively, in two other clades, AG-4 and AG-1 (Pattathil et al., 2010). There is some evidence that JIM8 may recognize residues in the galactan backbone, perhaps connected to arabinose or rhamnose (Pennell et al., 1991), whereas the JIM15 epitope might include glucuronic acid (Yates et al., 1996). AGPs are believed to be some of the most complex macropolymers in plant cells due to their strikingly high structural diversity (Majewska-Sawka and Rodriguez-Garcia, 2006; Ellis et al., 2010; Knoch et al., 2014), and have been previously shown, with the help of the *upex1/kns4* mutant, to be components of the developing pollen surface (Suzuki et al., 2017). Our results suggest that the increased presence of AGPs in *tex2* primexine may affect its layout and prevent the formation of probaculae and protectum.

Differences between *tex2* and other primexine mutants

Several mutants with defects in primexine formation (*dex1*, *nef1*, *nerd1*, *npu*, *rpg1*) have been previously identified in Arabidopsis (Paxson-Sowders et al., 2001; Ariizumi et al., 2004; Guan et al., 2008; Chang et al., 2012; Xu et al., 2020). It is noteworthy that unlike *tex2*, which, despite its very thin exine, still produces viable and fertile pollen, all these other mutants are pollen-lethal, with their microspores degrading soon after the release from tetrads. All the above mentioned primexine mutants also exhibit problems with the plasma

membrane undulation. Yet, in *tex2*, the membrane undulates normally, which shows that defects in the primexine formation and plasma membrane undulation can be separated. A particularly striking difference between the other primexine-deficient mutants and *tex2* is that the former all showed large (~1–3 μm) aggregates of sporopollenin near the surface of free microspores and in the anther locule (Paxson-Sowders et al., 1997, 2001; Ariizumi et al., 2004; Guan et al., 2008; Chang et al., 2012; Xu et al., 2020). In contrast, only small globules of sporopollenin (~100 nm) were found floating around the free microspores in *tex2*, while very large inclusions of sporopollenin-like material were sequestered inside the tapetal cells. This suggests that TEX2 may be required not only for formation of primexine, but also for sporopollenin transport out of tapetum. *tex2* also has noticeable differences from *spg2/irx9l* and *upex1/kns4*, the two mutants with abnormal primexine composition and with defects, respectively, in the formation of xylan and AGPs (Li et al., 2017; Suzuki et al., 2017). Like *tex2*, both these mutants have viable pollen. Their defects, however, appear to be milder than in *tex2*, as they are capable of forming probaculae and protectum and assembling sporopollenin into exine elements (Suzuki et al., 2008, 2017; Dobritsa et al., 2011; Li et al., 2017), and, importantly, they do not accumulate tapetal inclusions.

Accumulation of *tex2* inclusions requires normal sporopollenin biosynthesis

Tapetal inclusions represent the most prominent defect in the *tex2* anthers. Interestingly, such inclusions had not been reported so far in other mutants with deficient pollen wall development. In *tex2*, the inclusions first appear in tapetal cells when microspores are released from tetrads. After tapetal degeneration, the *tex2* inclusions remain in the anther locules and, during anther dehiscence, they are released, along with pollen grains, to the anther surface. Various tests that we performed on the *tex2* inclusions revealed their similarity to exine. Thus, it is likely that the *tex2* inclusions consist of a sporopollenin-like material. There are, however, differences in the autofluorescence spectra between the *tex2* inclusions and exine, suggesting that the two materials, while similar, are not identical. Since inclusions accumulate before the mature exine develops, it is possible that inclusions are made of sporopollenin precursors/immature sporopollenin. Also, sporopollenin assembly into tapetal inclusions might differ from the way it assembles and polarizes on the pollen surface, potentially leading to structural differences that may account for distinct autofluorescence spectra.

The sporopollenin biosynthesis pathway is fairly well established, with multiple genes already identified and characterized. Most of these genes are expressed specifically in tapetum, indicating that biosynthesis of exine components starts in tapetal cells, and their expression peaks during tetrad development (Lallemand et al., 2013; Quilichini et al., 2015; Wang et al., 2018). The *tex2* inclusions first appear in the tapetum immediately after the tetrad stage, suggesting a connection between sporopollenin synthesis and inclusion accumulation. This connection was confirmed by the double mutants between *tex2* and mutations disrupting the sporopollenin pathway, in which inclusions disappeared, demonstrating that accumulation of the *tex2* inclusions requires the intact sporopollenin biosynthesis.

A connection exists between *tex2* inclusions and sporopollenin transport

A particularly intriguing finding is that the accumulation of *tex2* inclusions is also suppressed by the loss of the *ABCG26* function. After the sporopollenin precursors are synthesized in tapetum, they need to be secreted into locules, delivered to developing microspores, and assembled into exine on the microspore surfaces. Transport of sporopollenin precursors out of the tapetum is poorly understood, but ABCG26, a plasma membrane-localized ABC transporter, is considered a major transporter for the polyketide precursors of sporopollenin (Quilichini et al., 2010, 2014b; Choi et al., 2011; Dou et al., 2011). In the *abcg26* mutant, small autofluorescent inclusions relying on the sporopollenin polyketide biosynthesis pathway accumulate in the vacuoles of tapetal cells (Quilichini et al., 2014b). The *abcg26* inclusions are different from *tex2* inclusions and do not require functional TEX2. Our findings that the *tex2* inclusions depend on the activity of ABCG26, but not vice versa, suggest that the step in exine formation that requires TEX2 is downstream of the step involving ABCG26. The TEX2-dependent step could be the sporopollenin assembly on the young microspore surface, for which formation of normal primexine likely serves as a prerequisite. The location of the *tex2* inclusions, however, presents an interesting conundrum: if the function of ABCG26 is indeed to transport polyketide sporopollenin precursors out of tapetum, then the accumulation of the *ABCG26*-dependent inclusions within the *tex2* tapetal cells suggests that the modified sporopollenin precursors travel back into tapetum. Quilichini et al. (2014b) proposed that the products of the polyketide biosynthesis pathway exported from tapetum by ABCG26 combine with hydroxycinnamoyl spermidines in the anther locule prior to being incorporated into developing exine. Thus, it could be that the *tex2* inclusions represent the hydroxycinnamoyl spermidine-modified version of the ABCG26-transported polyketides. However, whether the return of these compounds into tapetum represents a normal step in the sporopollenin biosynthesis or is something that happens in *tex2* because these compounds fail to assemble into exine will require further investigation. Yet, as mentioned earlier, the unassembled sporopollenin in other primexine mutants remains in the locule, not in tapetum (Paxson-Sowders et al., 1997, 2001; Ariizumi et al., 2004; Guan et al., 2008; Chang et al., 2012; Xu et al., 2020). This suggests that TEX2

is required not only for the assembly of sporopollenin but also for its export from tapetum.

tex2 inclusions and synthetic pollen lethality in double mutants can provide insights into interactions between genes and pathways involved in exine formation

The analysis of double mutants between *tex2* and sporopollenin biosynthesis genes has provided some other interesting insights. One of them concerns several sporopollenin biosynthesis genes (*CYP703A2*, *CYP704B1*, *MS2*, and *LAP6*), mutations in which affect exine development but not pollen viability (Morant et al., 2007; Dobritsa et al., 2009, 2010; Kim et al., 2010; Chen et al., 2011). When combined with *tex2*, the resulting double mutants develop synthetic pollen lethality, indicating strong genetic interactions between these sporopollenin biosynthesis genes and *TEX2* and suggesting that TEX2 and the products of the sporopollenin biosynthesis genes likely function in two separate genetic pathways that influence pollen viability.

Secondly, two of the sporopollenin biosynthesis-related genes, *TKPR2* and *LAP5*, behaved very differently from the other genes when their mutations were combined with *tex2*. Loss of *TKPR2* and *LAP5* functions failed to suppress the *tex2* inclusions or cause pollen lethality. The case of TKPR2 is perhaps not surprising, as it is likely to be a minor player in the exine formation (Grienenberger et al., 2010; Lallemand et al., 2013). Both TKPR2 and another protein with the similar *in vitro* tetraketide pyrone reductase activity, TKPR1, are co-expressed in tapetum, and, for this reason, are sometimes placed at the same position in the models of the sporopollenin biosynthesis pathway (Grienenberger et al., 2010; Quilichini et al., 2015; Shi et al., 2015). However, unlike TKPR1, which is associated with the ER and appears to be a member of the polyketide biosynthetic metabolon, TKPR2 is primarily localized to the cytosol and does not interact with the metabolon components (Grienenberger et al., 2010; Lallemand et al., 2013). Moreover, while *tkpr1* is pollen-lethal, the *tkpr2* defects are much milder, with plants producing viable pollen with only subtle changes in exine pattern (Grienenberger et al., 2010). It was previously suggested that TKPR1 and TKPR2 likely have different *in vivo* functions in pollen development (Grienenberger et al., 2010; Lallemand et al., 2013), and our data on genetic interactions of *TKPR2* and *TKPR1* with *TEX2* support this hypothesis.

In contrast, the case of LAP5 is more unexpected. *LAP5/PKSB* and its homolog *LAP6/PKSA* are highly co-expressed in tapetal cells and both encode ER-localized polyketide synthases (Dobritsa et al., 2010; Kim et al., 2010). As LAP5 and LAP6 have identical *in vitro* functions, both interact with ACOS5 and TKPR1, and their combined mutations synergistically disrupt pollen viability, they were proposed to have redundant functions in the potential ER-localized sporopollenin metabolon and occupy the same position in the sporopollenin pathway, despite some reported differences in their gene expression profiles and single-mutant exine phenotypes (Dobritsa et al., 2010; Grienenberger et al., 2010; Kim et al., 2010; Lallemand et al., 2013; Quilichini et al., 2015). In this study, we showed that, in its genetic interactions with *TEX2*, *LAP5* behaves very differently from *LAP6*. Unlike *lap6*, *lap5* does not suppress formation of *tex2* inclusions, nor causes pollen lethality in the double mutant. Furthermore, anthers in the *lap5* single mutant, but not in *lap6*, themselves accumulate *tex2*-like inclusions, indicating that the role of LAP5 in exine development is distinct from that of LAP6. LAP5 may function downstream of the other components of the sporopollenin pathway, or, like TEX2, it could be involved in other pathways required for exine development.

What is the function of TEX2?

TEX2 is a conserved plant protein that belongs to the family of NSTs (Dobritsa et al., 2011; Niemann et al., 2015; Niemann and Werner, 2015). These proteins transport nucleotide-charged monosaccharides from the cytosol into the ER and Golgi lumens where the sugar moieties become incorporated into polysaccharides, glycoproteins, and glycolipids (Rautengarten et al., 2014; Orellana et al., 2016). Therefore, TEX2, localized to the ER, is also expected to play a similar role, importing some sugar(s) into that compartment. Yet, which substrates are transported by TEX2 and how they are used in the ER is still unclear. The transporting activity of TEX2 has been previously studied using the yeast microsomal system, and it was found that TEX2 has some ability to transport the nucleotide-sugars UDP-GalNAc and UDP-GlcNAc (Niemann et al., 2015; Ebert et al., 2018). Although GalNAc is commonly used for mucin-type O-glycosylation in insects and mammals (Brockhausen et al., 2009; Tran and Ten Hagen, 2013), its role in plants is unknown (Strasser, 2016). Yet GlcNAc is incorporated—inside Golgi lumen—into N- and O-linked glycoproteins and into glycolipids (Strasser et al., 2005, 2016; Ishikawa et al., 2018). No glycosylation reactions involving GlcNAc in plants are presently known to occur in the ER lumen. Another Arabidopsis NST, UGNT1, was identified recently as a much more potent UDP-GlcNAc transporter compared with TEX2 (Ebert et al., 2018). Also, its subcellular localization (Golgi) and mutant phenotypes (significant loss of proteins and lipids with GlcNAc-containing glycosyl modifications) fit very well with the processes involving GlcNAc (Ebert et al., 2018). This provides support to the notion that UGNT1, and not TEX2, is the major transporter for UDP-GlcNAc in Arabidopsis. In this study, we created chimeric proteins of TEX2, with its transporting core replaced by that of UGNT1. Neither the chimeric proteins nor the intact UGNT1 guided by the *TEX2* promoter were able to rescue the *tex2* pollen phenotype, in agreement with the hypothesis that the *tex2* defects are not due to the abnormal transport of UDP-GlcNAc.

Our finding that expression of *TEX2* from the tapetum-specific *A9* promoter is sufficient to rescue the *tex2* exine defects indicates that tapetum—and not the developing pollen where *TEX2* is also expressed—is the site where TEX2

needs to be active to ensure proper exine development. Whether TEX2 from tapetum is involved in the primexine formation directly or indirectly is not clear. Although primexine develops underneath the layers of callose wall and the primary mother cell wall and was previously believed to be synthesized by the developing pollen, there is some recent evidence suggesting that primexine components might be coming from tapetum (Li et al., 2017). In that sense, the expected involvement of TEX2 in nucleotide-sugar transport might be directly relevant to the formation of polysaccharidic components of primexine. On the other hand, TEX2 was also proposed to play a role in the ER quality control (ERQC), a system that monitors proper protein folding in the secretory pathway (Niemann et al., 2015; Niemann and Werner, 2015). While the participation of TEX2 in ERQC has not yet been thoroughly investigated, if it functions in the same process in tapetum, then its involvement in exine formation is likely to be indirect, facilitated through some other protein(s) whose folding, stability, or activity are regulated by glycosylation.

Materials and methods

Plant materials and growth conditions

The Arabidopsis (*A. thaliana*) Col-0 ecotype served as the wild-type control. The T-DNA insertion alleles *tex2-3* (SALK_112086) and *tex2-2* (SALK_001259) were obtained from the Arabidopsis Biological Resource Center (ABRC, Columbus, OH). All the experiments were performed with *tex2-3*, unless otherwise noted. Seeds of the *rock1-1* allele of *TEX2* expressing P_{ROCK1}:*ROCK1-GFP*^{int} (Niemann et al., 2015) were kindly provided by Dr. Tomáš Werner (Freie Universität, Berlin). The P_{ROCK1}:*ROCK1-GFP*^{int} transgene (referred here to as P_{TEX2}:*TEX2-GFP*^{int}) was introduced into *tex2-3* by crossing. The T-DNA insertional mutants used for the analysis of *tex2* genetic interactions were obtained from ABRC. The homozygous insertion lines of SALK_119582 (*cyp703a2*), SAIL_1149_B03 (*cyp704b1*), SALK_079287 (*lap6*), GK_089C04/GK_454C04 (*lap5*), SAIL_75_E01 (*ms2*), SM3_37225 (*acos5*), SAIL_837_D01 (*tkpr1*), SALK_129453 (*tkpr2*), SALK_062317 (*abcg26*), GK_148H04 (*nef1*), SALK_124009 (*spg3/apy7*), SALK_037323 (*spg2/irx9l*), SALK_066961 (*irx14l*), and SALK_091466 (*upex1/kns4*) were identified by PCR with gene-specific and T-DNA left-border (LB)-specific primers (Supplemental Table S1). *dex1* [a T-DNA insertion allele in the Ws-2 background from the DuPont collection (Paxson-Sowders et al., 2001)] was kindly provided by Dr. Heather Owen (University of Wisconsin-Milwaukee). All plants were grown in growth chambers at 22°C under 16-h light/8-h dark cycle at the OSU Biotechnology greenhouse facility. Pollen survival in *tex2* could be sensitive to growth conditions (soil and light): Pro-Mix BRK W/ Mycorrhizae potting mix (#1020400, Hummert International, St. Louis, MO) supplemented with Ultrasol Multi-purpose Plus fertilizer, and F96T12 fluorescent lamps and 60-W incandescent bulbs providing the 120–150 μmol m^{-2} s^{-1} white light produced good results.

Confocal microscopy

Auramine O staining was performed as previously described (Reeder et al., 2016). Mature pollen grains were placed on a slide and stained with a drop of 0.001% (w/v) Auramine O solution (prepared from the stock solution of 0.1% (w/v) Auramine O in 50 mM Tris–HCl, pH 7.5). The rehydrated and stained pollen grains were examined with a Nikon A1+ laser scanning confocal microscope (100× objective, NA = 1.45). Exine was excited by the 488-nm laser and the signal was collected at 500–550 nm. In these and all other confocal imaging experiments, the parameters of laser power and gain were set up, respectively, at 5–25% and 75–140. The exact settings were chosen on a case-by-case basis to ensure that the signal was easily visible but not saturated. At least 50 pollen grains from a minimum of three independent plants were imaged in each case, with similar results.

To image the TEX2-GFP^{int} expression in anthers, anthers at different developmental stages were dissected from flower buds of the transgenic plants, mounted in Vectashield antifade solution (Vector Labs), and imaged with a Nikon A1+ laser scanning confocal microscope (40× objective, NA = 1.3; 100× objective, NA = 1.45). GFP was excited by the 488-nm laser and the signal was collected at 500–550 nm. Chlorophyll autofluorescence was excited by the 640-nm laser and the signal was collected at 663–738 nm. Experiments were repeated three times, with similar results.

To examine *abcg26* inclusions, the anthers with free microspores were collected, immersed in distilled water on a slide with the adaxial side facing up, covered with a #1.5 cover slip and sealed with nail polish. The anthers were examined with a Nikon A1+ laser scanning confocal microscope (100× objective, NA = 1.45). To identify the tapetal layer, the epidermal and endothecial layers were first identified in the brightfield channel; tapetum is the layer underneath. To determine the tapetal focus, chlorophyll autofluorescence from the endothecium [excitation at 640 nm (15% laser power), emission at 663–738 nm] was examined simultaneously with the tapetal intrinsic fluorescence, as tapetal cells lack chloroplasts. The tapetal intrinsic fluorescence was excited with the 405-nm laser (25% laser power) and the signal was collected at 500–550 nm. Experiments were repeated three times, with similar results.

Brightfield imaging, Alexander staining, and acetolysis

To image pollen and abnormal inclusions with brightfield microscopy, mature anthers were dissected from the oldest unopened flower buds and mounted in 100% glycerol. For Alexander staining, the same-stage anthers were mounted in one drop of the Alexander solution, prepared as previously described (Alexander, 1969). A coverslip was placed on top and samples were sealed with nail polish. Staining was performed at 50°C for 5 h. At least 30 anthers collected from a minimum of three plants were imaged for each genotype,

with similar results. Acetolysis experiments were performed on anthers from opened flowers as previously described (Dobritsa et al., 2009). Samples were imaged with Nikon Eclipse E600 (20× objective, NA = 0.5). To measure the sizes of pollen grains and inclusions, they were scraped from dehiscent anthers, put on a slide in a drop of 100% glycerol, covered with a coverslip, and sealed with nail polish. Samples from six plants per genotype were imaged with Nikon Eclipse E600 (100× objective, NA = 1.3), as shown in Figure 9, G and H. The area measurements for inclusions and pollen grains were performed with ImageJ.

Light microscopy and TEM of anther sections

To examine anther and pollen cross sections, the whole main inflorescences from four plants for each genotype were fixed in 2.5% (v/v) glutaraldehyde, 1% (v/v) Triton X-100, 0.1 M HEPES, pH 7.2 at room temperature overnight, followed by overnight post-fixation with 1% (v/v) osmium tetroxide. The samples were dehydrated by using a graded series of 10% increments of acetone, with a minimum of 1 h between changes. Acetone was then replaced with Spurr's resin by using a graded series of 20% increments of resin, with a minimum of 3 h between changes. The resin-infiltrated flower buds were then separated, labeled according to their order in the inflorescence, and individually embedded in the Spurr's resin. For light microscopy, 0.5-µm anther cross sections were cut using an Ultracut E ultramicrotome (Reichert-Jung). The sections were stained with 1% (w/v) Toluidine Blue O and imaged with a Nikon Eclipse E600 (20× objective, NA = 0.5). For TEM, silver sections (70 nm) were cut, stained with 1% (w/v) uranyl acetate followed by Reynold's lead citrate. Sections were imaged using a FEI Tecnai G2 Spirit TEM operating at 80 kV at the OSU Campus Microscopy and Imaging Facility (CMIF).

Scanning electron microscopy

Dehiscent anthers and dried pollen grains were collected from opened flowers and attached to the SEM stubs (Ted Pella) by using a double-sided carbon tape (Ted Pella). Samples were coated with gold using a Pelco Sputter Coater and imaged with a FEI Quanta 200 SEM at the OSU Center for Electron Microscopy and Analysis (CEMAS). Experiments were repeated twice, with similar results.

Spectral analysis of autofluorescence

Mature pollen grains were collected from dehiscent anthers and mounted in 100% glycerol. Samples were first illuminated with the 488-nm laser to adjust the focus on the surface of exine or inclusions. The spectral analysis was performed using a Nikon A1+ laser scanning confocal microscope (100× objective, NA = 1.45) with the 405-nm laser excitation (50% laser power) and collected with a spectral detector ($n = 20$ for both pollen grains and inclusions). The set of spectral images was recorded in sequential bandwidths of 10 nm, spanning the wavelength range between 410 and 620 nm. The signal intensities for exine and inclusions were normalized, respectively, to the intensities of their 430-nm and 460-nm peaks and mean and SE values were calculated.

TEX2 transient expression in *N. benthamiana* leaves

To create the P_{35S}:*TEX2*-YFP construct, the *TEX2* gene without the stop codon was amplified from the Col-0 genomic DNA with primers 15 and 16 (all primers used for making constructs are listed in Supplemental Table S2). In-Fusion cloning (Takara) was used to place this fragment along with the 2 × 35S promoter (amplified from pCAMBIA1380) into the *Age*I and *Nco*I sites of the T-DNA vector pGR111 (Dobritsa et al., 2010) upstream of *YFP*. To create the P_{35S}:*YFP-TEX2* construct, the *YFP* in pGR111 was replaced with *YFP* without the stop codon. The genomic fragment containing the whole coding region of *TEX2* was amplified from the Col-0 genomic DNA with primers 3 and 4. The fragment was placed via In-Fusion cloning downstream of the 2 × 35S promoter and *YFP* into the *Spe*I site of the modified pGR111. ER-rk and Golgi-rk (Nelson et al., 2007) were used, respectively, as markers for ER and Golgi localization. Constructs were individually transformed into the *Agrobacterium tumefaciens* strain GV3101. Agrobacteria were collected and resuspended in the infiltration buffer (10 mM $MgCl_2$, 10 mM MES, 150 µM acetosyringone) at the final concentration of OD_{600} = 0.1. Suspensions containing the *TEX2* constructs, the localization markers, and the RNA silencing suppressor P19 were combined and co-infiltrated into young *N. benthamiana* leaves and grown for 2–3 d in light. Epidermal cells were imaged using a Nikon A1+ confocal microscope (100× objective, NA = 1.45). YFP and mCherry were excited, respectively, by the 514-nm and 561-nm lasers, and the signals were collected simultaneously at 554 nm (YFP) and 580–630 nm (mCherry). Experiments were repeated three times, with similar results.

Immunofluorescence labeling

Whole main inflorescences from seven to eight plants per genotype were fixed in 2.5% (v/v) glutaraldehyde, 1% (v/v) Triton X-100, 0.1 M HEPES, pH 7.2 at room temperature overnight. Dehydration was then performed by using a graded series of 10% increments of ethanol, with a minimum of 1 h between changes. The ethanol was replaced with LR White resin (hard grade; Ted Pella) by using a graded series of 20% increments of resin, with a minimum of 3 h between changes. The resin-infiltrated inflorescences were separated into individual flower buds, which were labeled according to their order in the inflorescence. Individual buds were then embedded into LR White resin in gelatin capsules. For immunofluorescence labeling, 0.4-µm-thick sections were cut by using an Ultracut E ultramicrotome (Reichert-Jung). Sections were put on the 21-well Teflon-coated slide (EMS) and blocked with 3% (w/v) nonfat milk in 1× phosphate-buffered saline (PBS), pH 7.4 at room temperature for 1 h. Primary antibodies were diluted in the blocking solution and sections were incubated with antibodies for 4 h at room temperature, after which they were washed 10 times in 1× PBS. The rat mAbs LM10 and

LM11 (Megazyme) were used at 1:100 dilution. The rat mAbs JIM4, JIM5, JIM7, JIM8, JIM13, JIM15, JIM17, JIM20, and MAC207 (CarboSource Service) were used at 1:40 dilution. Secondary antibody (goat anti-rat-Alexa 488, Thermo Fisher) was diluted 1:100 in the blocking solution, and sections were incubated with the secondary antibody for 2 h at room temperature. After washing them 10 times with 1× PBS, the sections were mounted in Vectashield antifade solution (Vector Labs) containing 0.02% (w/v) Calcofluor White. Sections were examined with Nikon A1+ confocal microscope (100× objective, NA = 1.45). Alexa 488 and Calcofluor White were sequentially excited by the 488-nm and 405-nm lasers, and signals were collected separately at 500–550 nm (Alexa 488) and 450 nm (Calcofluor White). To compare labeling strength of JIM8 and JIM15 in different mutants, all images for the same antibody were captured with the same acquisition settings. All experiments were repeated at least twice, with similar results.

Transgenic constructs and plant transformation

To create the P_{A9}:*TEX2* construct, the *A9* promoter and the *TEX2* gene were amplified from the Col-0 genomic DNA with primer pairs 1/2, and 3/4, respectively. The fragments were then combined with the help of the In-Fusion HD Cloning Kit (Takara) in the pGR111 vector from which the *YFP* gene was removed. To create the P_{TEX2}:*UGNT1*, P_{TEX2}:*UGNT1*$^{\Delta C}$-*TEX2*^{C}, and P_{TEX2}:*TEX2*^{N}-*UGNT1*$^{\Delta N\Delta C}$-*TEX2*^{C} constructs, the genomic fragment containing the *TEX2* promoter (1,830 bp) was amplified with the primers 5 and 6. The topology of the TEX2 and UGNT1 proteins (positions of the N-terminal regions, C-terminal regions, and transmembrane regions) was predicted with the help of the Protein Homology/analogy Recognition Engine V 2.0 (Phyre^2; Kelley et al., 2015) and the Plant Membrane Protein Database ARAMEMNON (Schwacke et al., 2003). The *UGNT1* coding sequence (CDS) was amplified with primers 7 and 8 from Col-0 cDNA. To swap the UGNT1 C-terminal tail with that of TEX2 (*UGNT1*$^{\Delta C}$-*TEX2*^{C} construct), the corresponding fragments of *UGNT1* $^{\Delta C}$ and *TEX2*^{C} were amplified with the primers 7, 9, 10, and 11. To replace both the N-terminal and the C-terminal tails of UGNT1 with the corresponding tails of TEX2 (*TEX2*^{N}-*UGNT1*$^{\Delta N\Delta C}$-*TEX2*^{C} construct), PCR amplification with primers 11–14 from the *UGNT1*$^{\Delta C}$-*TEX2*^{C} construct was performed. The fragments were then placed through the In-Fusion cloning into the *Age*I site in pGR111 from which the *YFP* gene was removed. The constructs were verified by sequencing and transformed into the *A. tumefaciens* strain GV3101. *tex2-3* plants were transformed via the floral dip (Clough and Bent, 1998) and transgenic plants were selected with the BASTA herbicide. At least eight T_1 plants were obtained and analyzed for each construct, with similar results.

Accession numbers

The Arabidopsis Genome Initiative accession numbers for the genes used in this study are the following: At5g65000 (*TEX2/ROCK1*), At1g01280 (*CYP703A2*), At1g69500 (*CYP704B1*), At1g02050 (*LAP6/PKSA*), At4g34850 (*LAP5/PKSB*), At3g11980 (*MS2*), At1g62940 (*ACOS5*), At4g35420 (*TKPR1*), At1g68540 (*TKPR2*), At3g13220 (*ABCG26*), At3g09090 (*DEX1*), At5g13390 (*NEF1*), At4g19180 (*SPG3/APY7*), At1g27600 (*SPG2/IRX9L*), At5g67230 (*IRX14L*), At4g32272 (*UGNT1*), and At1g33430 (*UPEX1/KNS4*).

Supplemental data

Supplemental Table S1. Primers used for genotyping

Supplemental Table S2. Primers used for cloning

Supplemental Figure S1. Diagram of the *TEX2* gene structure with the positions of the three mutations used in this study.

Supplemental Figure S2. Larger versions of images shown as insets in Figure 1.

Supplemental Figure S3. TEM images of the abnormal inclusions in *tex2* anthers.

Supplemental Figure S4. Abnormal inclusions in the *tex2-2* allele.

Supplemental Figure S5. The larger versions of images of anthers from sporopollenin-related single mutants shown as insets in Figure 5.

Supplemental Figure S6. The accumulation of abnormal inclusions in *tex2* was suppressed by mutations in sporopollenin biosynthesis- or transport-related genes.

Supplemental Figure S7. The accumulation of *tex2* inclusions was not affected in *tex2 dex1* and *tex2 nef1*.

Supplemental Figure S8. Abnormal inclusions in *lap5* and *lap5 tex2* mutants involving a second allele of *lap5* (GK_454C04).

Supplemental Figure S9. Like *tex2*, *lap5* produces pollen with abnormally thin exine, while the double *tex2 lap5* mutant has more severe exine defects than either of the single mutants.

Supplemental Figure S10. The abnormal exine phenotype in the *rock1-1* allele of *TEX2* is rescued by the P_{TEX2}::*TEX2-GFP*^{int} transgenic construct.

Supplemental Figure S11. TEX2 is localized to the ER, although its subcellular localization can be affected by the position of the fluorescent protein tag.

Supplemental Figure S12. Schematic structures of TEX2, UGNT1, and two chimeric proteins.

Supplemental Figure S13. Staining of anthers at the tetrad stage of development with additional antibodies against AGPs.

Supplemental Figure S14. Enlarged views of tetrad-stage microspores stained for AGPs with JIM8 and JIM15 antibodies and presented in Figures 8, 10.

Supplemental Figure S15. Larger versions of images of anthers from single mutants of the carbohydrate-related exine-patterning genes shown as insets in Figure 9.

Supplemental Figure S16. Pollen grain development is disrupted in the *tex2 spg3* double mutant, but the abnormal inclusions are not suppressed.

Supplemental Figure S17. The double *tex2 upex1* mutant has more severe exine defects than either of the single mutants.

Acknowledgments

The authors are grateful to members of the Dobritsa Laboratory for discussions, to Sarah Reeder for critical reading of the manuscript, and to Dr. Heather Owen (University of Wisconsin, Milwaukee) for advice on TEM and for *dex1* seeds. They also thank the Arabidopsis Biological Resource Center (OSU) and Dr. Tomáš Werner (Freie Universität, Berlin) for seed stocks, Campus Microscopy & Imaging Facility and CEMAS at OSU for access to imaging equipment, and the NCI-subsidized Genomics Facility at the OSU Comprehensive Cancer Center (CCSG: P30 CA016058) for sequencing.

Funding

This work was supported by the US National Science Foundation (MCB-1817835) and the Department of Molecular Genetics at OSU to A.A.D. and by the Herta Camerer Gross Postdoctoral Research Fellowship to R.W.

Conflict of interest statement. The authors declare that they have no competing interests.

References

Aarts MG, Hodge R, Kalantidis K, Florack D, Wilson ZA, Mulligan BJ, Stiekema WJ, Scott R, Pereira A (1997) The Arabidopsis MALE STERILITY 2 protein shares similarity with reductases in elongation/condensation complexes. Plant J **12**: 615–623

Alexander MP (1969) Differential staining of aborted and nonaborted pollen. Stain Technol **44**: 117–122

Ariizumi T, Hatakeyama K, Hinata K, Inatsugi R, Nishida I, Sato S, Kato T, Tabata S, Toriyama K (2004) Disruption of the novel plant protein NEF1 affects lipid accumulation in the plastids of the tapetum and exine formation of pollen, resulting in male sterility in Arabidopsis thaliana. Plant J **39**: 170–181

Ariizumi T, Toriyama K (2011) Genetic regulation of sporopollenin synthesis and pollen exine development. Annu Rev Plant Biol **62**: 437–460

de Azevedo Souza C, Kim SS, Koch S, Kienow L, Schneider K, McKim SM, Haughn GW, Kombrink E, Douglas CJ (2009) A novel fatty Acyl-CoA synthetase is required for pollen development and sporopollenin biosynthesis in Arabidopsis. Plant Cell **21**: 507–525

Blackmore S, Wortley AH, Skvarla JJ, Rowley JR (2007) Pollen wall development in flowering plants. New Phytol **174**: 483–498

Brockhausen I, Schachter H, Stanley P (2009) O-GalNAc glycans. *In* A Varki, RD Cummings, JD Esko, Stanley P, Hart W, Aebi M, Darvill AG, Kinoshita T, Packer NH, Prestegard JH, **et al.**, eds, Essentials of Glycobiology. Ed 2, Chapter 9, Cold Spring Harbor Laboratory Press, Cold Spring Harbor, NY

Chang H-S, Zhang C, Chang Y-H, Zhu J, Xu X-F, Shi Z-H, Zhang X-L, Xu L, Huang H, Zhang S, et al. (2012) NO PRIMEXINE AND PLASMA MEMBRANE UNDULATION is essential for primexine deposition and plasma membrane undulation during microsporogenesis in Arabidopsis. Plant Physiol **158**: 264–272

Chen W, Yu X-H, Zhang K, Shi J, Oliveira SD, Schreiber L, Shanklin J, Zhang D (2011) Male Sterile2 encodes a plastid-localized fatty acyl carrier protein reductase required for pollen exine development in Arabidopsis. Plant Physiol **157**: 842–853

Chiu T-Y, Christiansen K, Moreno I, Lao J, Loqué D, Orellana A, Heazlewood JL, Clark G, Roux SJ (2012) AtAPY1 and AtAPY2 function as Golgi-localized nucleoside diphosphatases in *Arabidopsis thaliana*. Plant Cell Physiol **53**: 1913–1925

Choi H, Jin J-Y, Choi S, Hwang J-U, Kim Y-Y, Suh MC, Lee Y (2011) An ABCG/WBC-type ABC transporter is essential for transport of sporopollenin precursors for exine formation in developing pollen. Plant J **65**: 181–193

Clausen MH, Willats WGT, Knox JP (2003) Synthetic methyl hexagalacturonate hapten inhibitors of anti-homogalacturonan monoclonal antibodies LM7, JIM5 and JIM7. Carbohydr Res **338**: 1797–1800

Clough SJ, Bent AF (1998) Floral dip: a simplified method for Agrobacterium-mediated transformation of *Arabidopsis thaliana*. Plant J **16**: 735–743

Dobritsa AA, Geanconteri A, Shrestha J, Carlson A, Kooyers N, Coerper D, Urbanczyk-Wochniak E, Bench BJ, Sumner LW, Swanson R, et al. (2011) A large-scale genetic screen in Arabidopsis to identify genes involved in pollen exine production. Plant Physiol **157**: 947–970

Dobritsa AA, Lei Z, Nishikawa S, Urbanczyk-Wochniak E, Huhman DV, Preuss D, Sumner LW (2010) LAP5 and LAP6 encode anther-specific proteins with similarity to chalcone synthase essential for pollen exine development in Arabidopsis. Plant Physiol **153**: 937–955

Dobritsa AA, Shrestha J, Morant M, Pinot F, Matsuno M, Swanson R, Møller BL, Preuss D (2009) CYP704B1 is a long-chain fatty acid ω-hydroxylase essential for sporopollenin synthesis in pollen of Arabidopsis. Plant Physiol **151**: 574–589

Dou X-Y, Yang K-Z, Zhang Y, Wang W, Liu X-L, Chen L-Q, Zhang X-Q, Ye D (2011) WBC27, an adenosine tri-phosphate-binding cassette protein, controls pollen wall formation and patterning in Arabidopsis. J Integr Plant Biol **53**: 74–88

Ebert B, Rautengarten C, McFarlane HE, Rupasinghe T, Zeng W, Ford K, Scheller HV, Bacic A, Roessner U, Persson S, et al. (2018) A Golgi UDP-GlcNAc transporter delivers substrates for N -linked glycans and sphingolipids. Nat Plants **4**: 792–801

Ellis M, Egelund J, Schultz CJ, Bacic A (2010) Arabinogalactan-proteins: key regulators at the cell surface? Plant Physiol **153**: 403–419

Erdtman G (1952) Pollen morphology and plant taxonomy. Geol Fören Stock För **74**: 526–527

Erdtman G (1969) Handbook of Palynology: Morphology, Taxonomy, Ecology. An Introduction to the Study of Pollen Grains and Spores. Munksgaard, Copenhagen

Erdtman G (1960) The acetolysis method: a revised description. Sven Bot Tidskr **54**: 561–564

Feng X, Dickinson HG (2010) Tapetal cell fate, lineage and proliferation in the Arabidopsis anther. Development **137**: 2409–2416

Gabarayeva NI, Grigorjeva VV (2021) An integral insight into pollen wall development: involvement of physical processes in exine ontogeny in *Calycanthus floridus* L., with an experimental approach. Plant J **105**: 736–753

Gabarayeva NI, Grigorjeva VV, Lavrentovich MO (2020) Artificial pollen walls simulated by the tandem processes of phase separation and self-assembly in vitro. New Phytol **225**: 1956–1973

Grienenberger E, Kim SS, Lallemand B, Geoffroy P, Heintz D, Souza C de A, Heitz T, Douglas CJ, Legrand M (2010) Analysis of TETRAKETIDE α-PYRONE REDUCTASE function in Arabidopsis thaliana reveals a previously unknown, but conserved, biochemical pathway in sporopollenin monomer biosynthesis. Plant Cell **22**: 4067–4083

Guan Y-F, Huang X-Y, Zhu J, Gao J-F, Zhang H-X, Yang Z-N (2008) RUPTURED POLLEN GRAIN1, a member of the MtN3/saliva

gene family, is crucial for exine pattern formation and cell integrity of microspores in Arabidopsis. Plant Physiol **147**: 852–863

Heslop-Harrison J (1968) Wall development within the microspore tetrad of *Lilium longiflorum*. Can J Bot **46**: 1185–1192

Hu J, Wang Z, Zhang L, Sun M (2014) The Arabidopsis exine formation defect (EFD) gene is required for primexine patterning and is critical for pollen fertility. New Phytol **203**: 140–154

Ishikawa T, Fang L, Rennie EA, Sechet J, Yan J, Jing B, Moore W, Cahoon EB, Scheller HV, Kawai-Yamada M, et al. (2018) GLUCOSAMINE INOSITOLPHOSPHORYLCERAMIDE TRANSFERASE1 (GINT1) is a GlcNAc-containing glycosylinositol phosphorylceramide glycosyltransferase. Plant Physiol **177**: 938–952

Kelley LA, Mezulis S, Yates CM, Wass MN, Sternberg MJE (2015) The Phyre2 web portal for protein modeling, prediction and analysis. Nat Protoc **10**: 845–858

Kim SS, Grienenberger E, Lallemand B, Colpitts CC, Kim SY, Souza C de A, Geoffroy P, Heintz D, Krahn D, Kaiser M, et al. (2010) LAP6/POLYKETIDE SYNTHASE A and LAP5/POLYKETIDE SYNTHASE B encode hydroxyalkyl α-pyrone synthases required for pollen development and sporopollenin biosynthesis in *Arabidopsis thaliana*. Plant Cell **22**: 4045–4066

Klepikova AV, Kasianov AS, Gerasimov ES, Logacheva MD, Penin AA (2016) A high resolution map of the *Arabidopsis thaliana* developmental transcriptome based on RNA-seq profiling. Plant J **88**: 1058–1070

Knoch E, Dilokpimol A, Geshi N (2014) Arabinogalactan proteins: focus on carbohydrate active enzymes. Front Plant Sci **5**: 198

Knox JP, Linstead PJ, Cooper JPC, Roberts K (1991) Developmentally regulated epitopes of cell surface arabinogalactan proteins and their relation to root tissue pattern formation. Plant J **1**: 317–326

Knox JP, Linstead PJ, King J, Cooper C, Roberts K (1990) Pectin esterification is spatially regulated both within cell walls and between developing tissues of root apices. Planta **181**: 512–521

Lallemand B, Erhardt M, Heitz T, Legrand M (2013) Sporopollenin biosynthetic enzymes interact and constitute a metabolon localized to the endoplasmic reticulum of tapetum cells. Plant Physiol **162**: 616–625

Li H, Kim Y-J, Yang L, Liu Z, Zhang J, Shi H, Huang G, Persson S, Zhang D, Liang W (2020) Grass-specific EPAD1 is essential for pollen exine patterning in Rice. Plant Cell **32**: 3961–3977

Li WL, Liu Y, Douglas CJ (2017) Role of glycosyltransferases in pollen wall primexine formation and exine patterning. Plant Physiol **173**: 167–182

Lim MH, Wu J, Yao J, Gallardo IF, Dugger JW, Webb LJ, Huang J, Salmi ML, Song J, Clark G, et al. (2014) Apyrase suppression raises extracellular ATP levels and induces gene expression and cell wall changes characteristic of stress responses. Plant Physiol **164**: 2054–2067

Lou Y, Zhu J, Yang Z (2014) Molecular cell biology of pollen walls. *In* P Nick, Z Opatrny, eds, Applied Plant Cell Biology: Cellular Tools and Approaches for Plant Biotechnology. Springer, Berlin, Heidelberg, pp 179–205

Ma L, Yang Z, Zhang S (2013) DEX1, a plasma membrane-localized protein, functions in microspore development by affecting CalS5 expression in *Arabidopsis thaliana*. Chin Sci Bull **58**: 2855–2861

Majewska-Sawka A, Rodriguez-Garcia MI (2006) Immunodetection of pectin and arabinogalactan protein epitopes during pollen exine formation of *Beta vulgaris* L. Protoplasma **228**: 41–47

McCartney L, Marcus SE, Knox JP (2005) Monoclonal antibodies to plant cell wall xylans and arabinoxylans. J Histochem Cytochem **53**: 543–546

Mondol PC, Xu D, Duan L, Shi J, Wang C, Chen X, Chen M, Hu J, Liang W, Zhang D (2020) Defective Pollen Wall 3 (DPW3), a novel alpha integrin-like protein, is required for pollen wall formation in rice. New Phytol **225**: 807–822

Morant M, Jørgensen K, Schaller H, Pinot F, Møller BL, Werck-Reichhart D, Bak S (2007) CYP703 is an ancient cytochrome P450 in land plants catalyzing in-chain hydroxylation of lauric acid to provide building blocks for sporopollenin synthesis in pollen. Plant Cell **19**: 1473–1487

Nelson BK, Cai X, Nebenführ A (2007) A multicolored set of in vivo organelle markers for co-localization studies in Arabidopsis and other plants. Plant J **51**: 1126–1136

Niemann MCE, Bartrina I, Ashikov A, Weber H, Novák O, Sp´chal L, Strnad M, Strasser R, Bakker H, Schmülling T, et al. (2015) Arabidopsis ROCK1 transports UDP-GlcNAc/UDP-GalNAc and regulates ER protein quality control and cytokinin activity. Proc Natl Acad Sci USA **112**: 291–296

Niemann MCE, Werner T (2015) Endoplasmic reticulum: Where nucleotide sugar transport meets cytokinin control mechanisms. Plant Signal Behav **10**: e1072668

Orellana A, Moraga C, Araya M, Moreno A (2016) Overview of nucleotide sugar transporter gene family functions across multiple species. J Mol Biol **428**: 3150–3165

Owen HA, Makaroff CA (1995) Ultrastructure of microsporogenesis and microgametogenesis in *Arabidopsis thaliana* (L.) Heynh. ecotype Wassilewskija (Brassicaceae). Protoplasma **185**: 7–21

Pattathil S, Avci U, Baldwin D, Swennes AG, McGill JA, Popper Z, Bootten T, Albert A, Davis RH, Chennareddy C, et al. (2010) A comprehensive toolkit of plant cell wall glycan-directed monoclonal antibodies. Plant Physiol **153**: 514–525

Paul W, Hodge R, Smartt S, Draper J, Scott R (1992) The isolation and characterisation of the tapetum-specific *Arabidopsis thaliana* A9 gene. Plant Mol Biol **19**: 611–622

Paxson-Sowders DM, Dodrill CH, Owen HA, Makaroff CA (2001) DEX1, a novel plant protein, is required for exine pattern formation during pollen development in Arabidopsis. Plant Physiol **127**: 1739–1749

Paxson-Sowders DM, Owen HA, Makaroff CA (1997) A comparative ultrastructural analysis of exine pattern development in wild-type Arabidopsis and a mutant defective in pattern formation. Protoplasma **198**: 53–65

Pennell RI, Janniche L, Kjellbom P, Scofield GN, Peart JM, Roberts K (1991) Developmental regulation of a plasma membrane arabinogalactan protein epitope in oilseed rape flowers. Plant Cell **3**: 1317–1326

Quilichini TD, Douglas CJ, Samuels AL (2014a) New views of tapetum ultrastructure and pollen exine development in *Arabidopsis thaliana*. Ann Bot **114**: 1189–1201

Quilichini TD, Friedmann MC, Samuels AL, Douglas CJ (2010) ATP-binding cassette transporter G26 is required for male fertility and pollen exine formation in Arabidopsis. Plant Physiol **154**: 678–690

Quilichini TD, Grienenberger E, Douglas CJ (2015) The biosynthesis, composition and assembly of the outer pollen wall: A tough case to crack. Phytochemistry **113**: 170–182

Quilichini TD, Samuels AL, Douglas CJ (2014b) ABCG26-mediated polyketide trafficking and hydroxycinnamoyl spermidines contribute to pollen wall exine formation in Arabidopsis. Plant Cell **26**: 4483–4498

Radja A, Horsley EM, Lavrentovich MO, Sweeney AM (2019) Pollen cell wall patterns form from modulated phases. Cell **176**: 856–868.e10

Rautengarten C, Ebert B, Moreno I, Temple H, Herter T, Link B, Doñas-Cofré D, Moreno A, Saéz-Aguayo S, Blanco F, et al. (2014) The Golgi localized bifunctional UDP-rhamnose/UDP-galactose transporter family of Arabidopsis. Proc Natl Acad Sci USA **111**: 11563–11568

Reeder SH, Lee BH, Fox R, Dobritsa AA (2016) A Ploidy-sensitive mechanism regulates aperture formation on the Arabidopsis pollen surface and guides localization of the aperture factor INP1. PLoS Genet **12**: e1006060

Rhee SY, Somerville CR (1998) Tetrad pollen formation in quartet mutants of *Arabidopsis thaliana* is associated with persistence of pectic polysaccharides of the pollen mother cell wall. Plant J **15**: 79–88

Roshchina VV (2012) Vital autofluorescence: application to the study of plant living cells. Int J Spectrosc **2012**: e124672

Ruprecht C, Bartetzko MP, Senf D, Dallabernadina P, Boos I, Andersen MCF, Kotake T, Knox JP, Hahn MG, Clausen MH, et al. (2017) A synthetic glycan microarray enables epitope mapping of plant cell wall glycan-directed antibodies. Plant Physiol **175**: 1094–1104

Sanders PM, Bui AQ, Weterings K, McIntire KN, Hsu Y-C, Lee PY, Truong MT, Beals TP, Goldberg RB (1999) Anther developmental defects in *Arabidopsis thaliana* male-sterile mutants. Sex Plant Reprod **11**: 297–322

Schwacke R, Schneider A, E van der Graaff, Fischer K, Catoni E, Desimone M, Frommer WB, Flügge U-I, Kunze R (2003) ARAMEMNON, a novel database for Arabidopsis integral membrane proteins. Plant Physiol **131**: 16–26

Scott RJ (1994) Pollen exine—the sporopollenin enigma and the physics of pattern. *In* RJ Scott and AD Stead, eds, Molecular and cellular aspects of plant reproduction. Cambridge University Press, Cambridge, UK, pp 49–81

Shi J, Cui M, Yang L, Kim Y-J, Zhang D (2015) Genetic and biochemical mechanisms of pollen wall development. Trends Plant Sci **20**: 741–753

Strasser R (2016) Plant protein glycosylation. Glycobiology **26**: 926–939

Strasser R, Stadlmann J, Svoboda B, Altmann F, Glössl J, Mach L (2005) Molecular basis of *N*-acetylglucosaminyltransferase I deficiency in *Arabidopsis thaliana* plants lacking complex *N*-glycans. Biochem J **387**: 385–391

Sun MX, Huang XY, Yang J, Guan YF, Yang ZN (2013) Arabidopsis RPG1 is important for primexine deposition and functions redundantly with RPG2 for plant fertility at the late reproductive stage. Plant Reprod **26**: 83–91

Suzuki T, Masaoka K, Nishi M, Nakamura K, Ishiguro S (2008) Identification of kaonashi mutants showing abnormal pollen exine structure in *Arabidopsis thaliana*. Plant Cell Physiol **49**: 1465–1477

Suzuki T, Narciso JO, Zeng W, van de Meene A, Yasutomi M, Takemura S, Lampugnani ER, Doblin MS, Bacic A, Ishiguro S (2017) KNS4/UPEX1: a Type II arabinogalactan β-(1,3)-galactosyltransferase required for pollen exine development. Plant Physiol **173**: 183–205

Tran DT, Ten Hagen KG (2013) Mucin-type *O*-glycosylation during development. J Biol Chem **288**: 6921–6929

Verhertbruggen Y, Marcus SE, Haeger A, Ordaz-Ortiz JJ, Knox JP (2009) An extended set of monoclonal antibodies to pectic homogalacturonan. Carbohydr Res **344**: 1858–1862

Wang K, Guo Z-L, Zhou W-T, Zhang C, Zhang Z-Y, Lou Y, Xiong S-X, Yao X, Fan J-J, Zhu J, et al. (2018) The regulation of sporopollenin biosynthesis genes for rapid pollen wall formation. Plant Physiol **178**: 283–294

Wang R, Dobritsa AA (2018) Exine and aperture patterns on the pollen surface: their formation and roles in plant reproduction. *In* JA Roberts, ed., Annual Plant Reviews. John Wiley & Sons, pp 1–40

Willats WGT, Steele-King CG, McCartney L, Orfila C, Marcus SE, Knox JP (2000) Making and using antibody probes to study plant cell walls. Plant Physiol Biochem **38**: 27–36

Xu D, Mondol PC, Ishiguro S, Shi J, Zhang D, Liang W (2020) NERD1 is required for primexine formation and plasma membrane undulation during microsporogenesis in *Arabidopsis thaliana*. aBIOTECH **1**: 205–218

Yang J, Wu J, Romanovicz D, Clark G, Roux SJ (2013) Co-regulation of exine wall patterning, pollen fertility and anther dehiscence by Arabidopsis apyrases 6 and 7. Plant Physiol Biochem **69**: 62–73

Yates EA, Valdor JF, Haslam SM, Morris HR, Dell A, Mackie W, Knox JP (1996) Characterization of carbohydrate structural features recognized by anti-arabinogalactan-protein monoclonal antibodies. Glycobiology **6**: 131–139

Yu J, Meng Z, Liang W, Behera S, Kudla J, Tucker MR, Luo Z, Chen M, Xu D, Zhao G, et al. (2016) A rice Ca^{2+} binding protein is required for tapetum function and pollen formation. Plant Physiol **172**: 1772–1786

Zinkl GM, Zwiebel BI, Grier DG, Preuss D (1999) Pollen-stigma adhesion in Arabidopsis: a species-specific interaction mediated by lipophilic molecules in the pollen exine. Development **126**: 5431–5440